ISSN. 2476-1234

Journal of Solar Energy Science And Research

Volume No. 9
Issue No. 2
May - August 2025

ENRICHED PUBLICATIONS PVT.LTD

JE - 18,Gupta Colony, Khirki Extn,
Malviya Nagar, New Delhi - 110017.
E- Mail: info@enrichedpublication.com
Phone :- +91-8877340707

ISSN. 2476-1234

Journal of Solar Energy Science And Research

Aims and Scope

The Journal of Solar Energy Science and Research is published quarterly by Enriched publications. Journal of Solar Energy Science and Research is peer reviewed journal and monitored by a team of reputed reviewers. Today, the journal continues to publish articles on topics ranging from solar radiation and solar materials to direct conversion of solar energy into electrical energy. In addition, readers will find important articles exploring other renewable energy sources. This journal places a strong emphasis on applications such as solar devices for home and industrial uses, solar heating and cooling systems, solar power systems and units, and agricultural uses of solar energy.

ISSN. 2476-1234

Journal of Solar Energy Science And Research

ISSN. 2476-1234

Journal of Solar Energy Science And Research

(Volume No. 8, Issue No. 2, May - August 2024)

Contents

ISSN. 2476-1234

Meta-Heuristic Optimization of the Neuro-Fuzzy MPPT Controller for PV Systems Under Partial Shading Conditions

Abena Malobé Paula, Djondiné Philippe a,b,*, Ntsama Eloundou Pascala,b

aDepartment of Physics, Faculty of Sciences, The University of Ngaoundéré, .O.Box 454 Ngaoundéré, Cameroon bDepartment of Physics, Higher Teacher Training college of Bertoua, The University of Bertoua, Cameroon

ABSTRACT

The main challenge of photovoltaic (PV) systems is to extract the maximum power from the array, especially when it is partially shaded and subjected to variable weather conditions (sunshine and temperature). To address this challenge, this manuscript proposes a new method based on the Neuro-Fuzzy- Particle Swarm Optimization (NF-PSO) combination. The NF method is used here because it allows an automatic generation of fuzzy rules, and we inject the PSO meta-heuristic at the input of the Neuro-fuzzy to find an optimal gain allowing not only to convert the real input values into fuzzy quantities and to readjust the dynamics of the fuzzy rules by reducing the power losses (oscillations), this combination also provides a simple and robust MPPT scheme to manage efficiently the partial shading, and its convergence to the global maximum power point (GMPP) is independent of the initial conditions of the search process. To confirm the NF-PSO as a viable MPPT option a comprehensive evaluation is performed against two other methods, namely the cuckoo algorithm and the original Neuro-Fuzzy. The simulation results of the system confirmed the better performance of this method in terms of speed with a response time of 0.044s, efficiency with 99.94%, and especially in terms of oscillation reduction with practically a negligible oscillation rate compared to the NF and the Cuckoo algorithm.

Keywords: *NF-PSO, Cuckoo, meta-heuristics, partial shading, GMPP*

1. Introduction

With the increasing demand for energy in the world, and the associated polluting effects, mainly caused by the combustion of fossil fuels that leads to global warming, the use of energy produced by renewable sources is becoming promptly a solution for the global energy plan [1, 2]. Among the renewable energies we have solar energy, which is currently the easiest energy system to install, the most reliable, the most abundant, and most importantly, with the advances in technology, a significant reduction in the costs of the components of this energy [2]. Notwithstanding these advantages, solar power systems have a major issue of optimizing energy recovery, which is why these systems must include maximum power point tracking (MPPT) controllers. In addition to that the power generated by PV modules depends on environmental factors, namely solar radiation and atmospheric temperature [3]. All these drawbacks affect the characteristic curves of a PV system, because for a constant irradiance the characteristic curves of a PV system have only one maximum power point (MPP), while for a varied irradiance like the partial shading of some cells, these curves have several MPPs, among which the

local points (LMPP) and the global point (GMPP). Therefore, an MPPT method must be able to extract the optimal power available under all operating conditions [4, 5]. This has motivated several researchers to focus on the development of MPPT methods capable of extracting the GMPP regardless of the operating conditions. In [2] Jubaer Ahmed et al present the Cuckoo Search (CS) algorithm; this algorithm is very efficient but has a convergence rate that is affected by the Levy flight and can be slower. Smail C. et al in [6], a new hybrid GWO-PSO method is proposed; in this hybridization, GWO search agents explore the search space deeply to avoid LMPPs, and thus can converge to GMPP and this exploration is controlled by the PSO algorithm, which in turn improves the solutions This exploration is controlled by the PSO algorithm, which in turn improves the obtained solutions as the process goes on in order to accelerate the convergence to GMPP in the exploitation phase. This method is efficient and converges quickly on the GMPP, but its concern is that it presents some oscillations in steady state which can lead to power losses. Similarly in [7], Makhloufi et al propose a global/local maximum power point tracker based on the logarithmic PSO for partially shaded PV systems. The authors of [8] recently improved the EGWO algorithm by adding a new wolf hopping procedure, they show that the developed EGWO can reduce the tracking time up to 45.5% and increase the dynamic efficiency by more than 2%, compared to the original GWO. In [9-10] the authors present an improved gray wolf algorithm; in [11] Eltamaly et al present a GWO hybridization with fuzzy logic controller (GWO-FLC). In [12, 13] respectively, perturb-and-observe (P & O), and incremental conductance (INC), presented known classical methods, the problem with these methods is that they are often trapped in a local maximum power point (LMPP) without reaching the GMPP. In [14-16], a modification of the P&O is performed and the defect of this method is that there is always the possibility that it is trapped in the LMPP. In [17] Claude Bertin N. et al made a comparative study between six MPPT methods, where they showed the superiority of fuzzy logic over the other five MPPT methods Fractional Short-Circuit Current (FSCC), Fractional Open-Circuit Voltage (FOCV), Perturb and Observe (P&O), Incremental Conductance (INC) and Hill Climbing (HC). In [18-20], respectively two modified methods HillClimbing (HC) and Incremental Conductance (INC) are presented, their disadvantage is that they require to perform several iterations. In [21], Özgür C. et al worked on a hybrid MPPT by combining Perturb and Observe and Artificial Neural Networks (P&O-RNA) methods; in [22] Alireza R. et al worked on a Fuzzy-Neural (FN) MPPT algorithm for PV. In [23] also Alireza Z. et al developed a partial shading algorithm for sensing that requires only the available measurements of row voltage and current. Ahmad R. et al in [24], they worked on Genetic Algorithm (GA) and PSO; all these hybridizations are known for their performance, but most of them still have steady state oscillations in the power output, which leads to power losses. In [25] Shams I. et al presented a modified butterfly optimization algorithm. In [26] Raeisi H. et al proposed a new set of relations to simulate the performance of a panel under partial shading conditions and a simulator is constructed accordingly.

Mazaheri Salehi et al in [27] presented a state of the art on mppt methods and their applications. In [28] Venkateswari R. et al carried out a critical analysis of the factors improving the efficiency of a photovoltaic solar system. In [29] Oulcaid M. et al show that so far very little attention has been paid to the evaluation of MPPT methods, so they develop a method that can improve the performance of an MPPT. In [30] Syafaruddin et al a MPPT system is proposed for a partially shaded PV generator using neural networks and fuzzy logic with a polar information controller. The main drawback of this method is the high cost and complexity, due to the combination of two intelligent methods. The objective of this manuscript is to introduce a PSO algorithm that improves the performance of NF. PSO readjusts the dynamics of the fuzzy rules in order to accelerate the convergence to the desired performance. Moreover, this hybridization allows the GMPP to be reached in only a few steps, thus making the MPPT controller more efficient.

This paper includes the following parts: the second section of the paper will be dedicated to the modeling of the PV generator and the boost converter. A third section is reserved for the presentation of the method used. The different simulations made as well as the discussion of the results found will be the subject of the fourth section. In the fifth section a conclusion is presented.

2. Materials and methods

2.1. Materials

In this part we present our studied system which consists of a Photovoltaic (PV) panel, and a boost converter.

2.1.1. Photovoltaic panel model

The scientific community offers several models to model a photovoltaic panel. The most widely used model, for its simplicity and accuracy, is the one with one diode [31] (Figure 1).

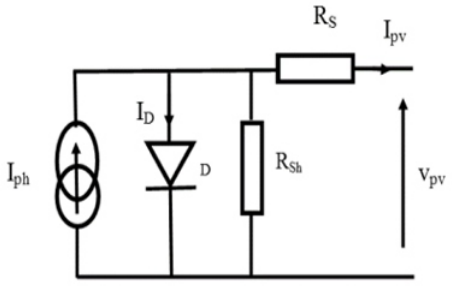

Figure 1. Single diode model of a PV cell

In this model, the photovoltaic cell is represented by a current source that generates a current Iph proportional to the solar radiation. The shunt resistance Rsh characterizes the leakage current at the junction and the resistance Rs represents the various contact and connection resistances. The current supplied by the cell Ipv is modeled by the following equation [32]:

$$I_{pv} = N_p I_{ph} - N_p I_0 \left[\exp\left(\frac{qV_{pv}}{N_s nKT}\right) - 1\right] \quad (1)$$

The inverse saturation current Io is:

$$Io = Ior \left(\frac{T}{Tr}\right)^3 \exp\left(\frac{qE_g}{nKT}\left(\frac{1}{Tr} - \frac{1}{T}\right)\right) \quad (2)$$

The inverse saturation current at Tr is:

$$Ior = \frac{I_{scr}}{exp\left(\frac{qV_{oc}}{nKTN_s}\right) - 1} \quad (3)$$

$$Iph = [I_{scr} + (K_i(T - Tr))]\frac{E}{100} \quad (4)$$

PV module power can therefore be obtained as follows:

$$P_{pv} = V_{pv} I_{pv} = N_p V_{pv} I_{ph} - V_{pv} N_p I_0 \left[\exp\left(\frac{qV_{pv}}{N_s nKT}\right) - 1\right] \quad (5)$$

Knowing that a PV generator has several PV modules associated in series and/or parallel, in our work, each PV generator consists of four Canadian Solar CS5C-80M modules connected in series. Figure 2 shows the four shaded PV arrays used in this paper. The electrical parameters under standard conditions (G= 1000W/m2, and T=25C°) of the PV module used for the simulations are presented in Table 1. Figure 3 shows the typical power-voltage and current-voltage curve for the shaded PV array.

Table 1. Parameters of PV

Parameters	Values
Maximum Power	80.15 W
Optimum operating voltage	17.5 V
Optimum operating current	4.58 A
Open circuit voltage	21.8 V
Schort-circuit current	4.97 A

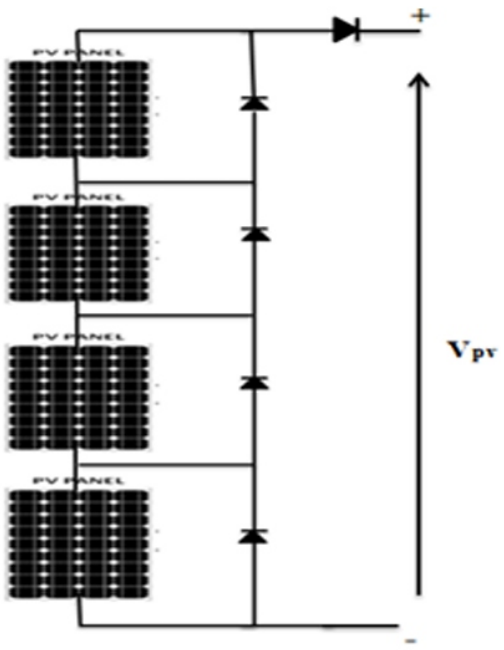

Figure 2. Structure of the PV array use

Table 2. Shading patterns used [5]

Pattern number	Irradiance variations (W/m2) for each sub-module				GMPP(W/m^2)
SP1	1000	1000	1000	1000	320.6
SP2	1000	500	1000	1000	236.7
SP3	1000	700	100	1000	183
SP4	1000	700	500	250	132

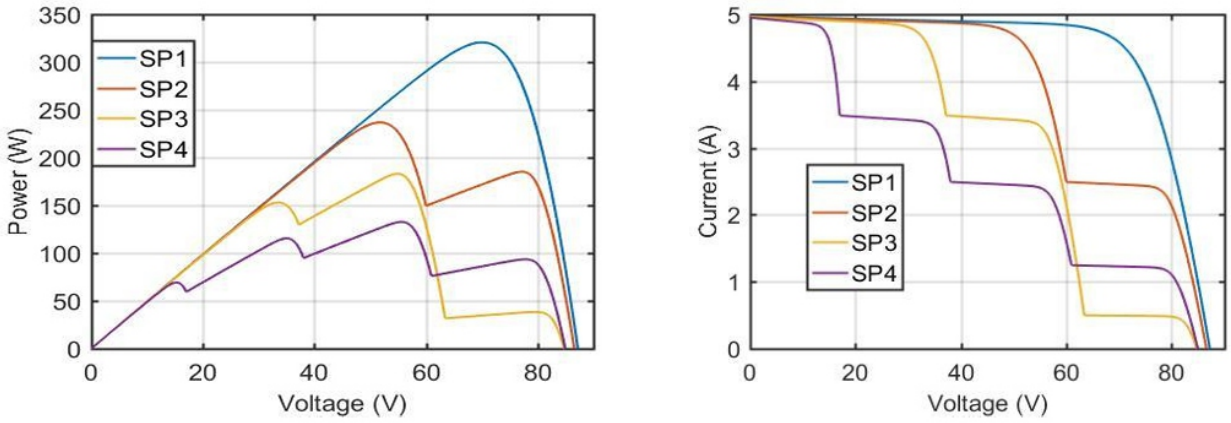

Figure 3. Power-Voltage and Current-Voltage characteristics of the models used

2.1.2. Boost converter

Static converters are essential parts of the variable speed wind power conversion system. In this document, a boost converter is used here. During operation of the chopper, the switch is closed with a closing time equal to (D.T), and it is opened in an opening time ((1-D) .T), with: T is the switching

period and D the duty cycle of the switch (D [0,1]).

$$V_{out} = \frac{V_{in}}{1-D} \quad (6)$$

Where:

V_{out}: Output voltage;

V_{in} : input voltage;

D: duty cycle.

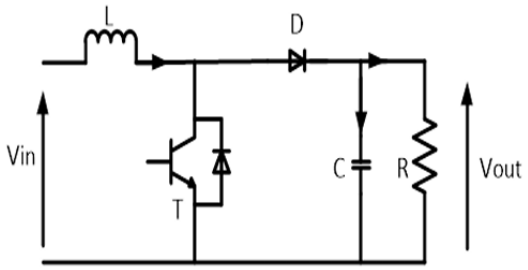

The converter parameters are given in table 3.

Table 3. Converter parameters

Parameters	Values
Load	30 Ω
Inductor	3 mH
Capacitor	100µF

2.2. Methods

In this section, we present the method used which consists of NF controller and the determination of offset gains by the PSO

2.2.1. NF Controller

The NF method developed here is based on the ANFIS (Adaptive Neuro-Fuzzy Inference System) model with the difference that our membership functions used here are triangular and not Gaussian. ANFIS implements a Takagi Sugeno type fuzzy inference system and has an architecture composed of five layers as shown in Figure 5 [33]. Our method contains two inputs: the error (E) and the variation of the error (ΔE), and a single output which is the variation of the duty cycle (D).

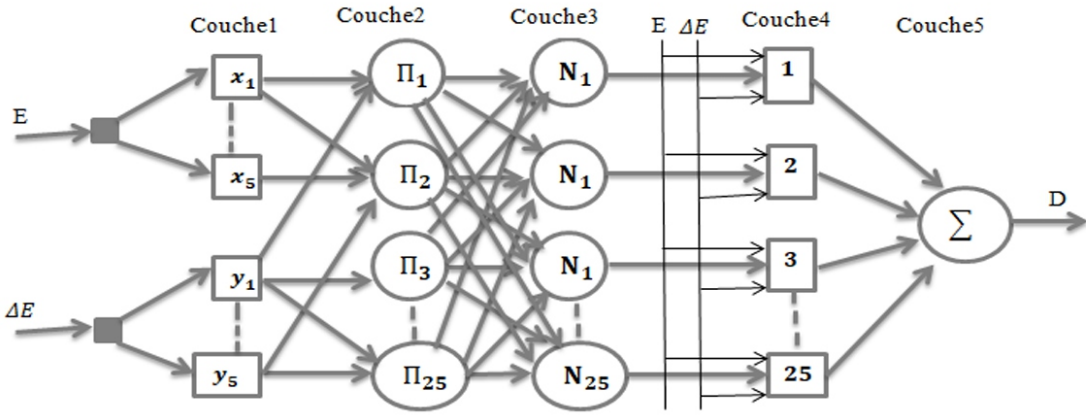

Figure 5. Architecture of ANFIS used.

The nodes of the input layer, whose number is equal to the number of linguistic terms (calculate the membership degrees of the input values by equations 7 and 8), forward the numerical data to the nodes of the second layer representing the fuzzy subsets that calculate the membership function value (equation 11). The nodes in the third layer perform the fuzzy operations (equation 12). The nodes of the fourth layer perform the operation of calculating the weighted consequent of the rule (equation 13) [33-34]. Finally the fifth layer (equation 14) performs the defuzzification operation.

$$o^1_{k_{x_i}} = \mu_{xi}(E)\ , \quad k_{x_i}=1,\ 2,\ 3,\ 4,\ 5 \tag{7}$$

$$x_i = MN, LN, Z, LP, MP$$

$$o^1_{k_{y_i}} = \mu_{yi}(\Delta E) \quad k_{y_i}=1,2,\ 3,\ 4,\ 5 \tag{8}$$

$$y_i = MN, LN, Z, LP, MP$$

$$E = \frac{I(k)-I(k-1)}{V(k)-V(k-1)} \tag{9}$$

$$\Delta E = E(k) - E(k-1) \tag{10}$$

Where E and are respectively the inputs of nodes and of layer1. and are the linguistic terms associated with membership functions and . In our case the linguistic terms used are Most Negative (MN), Least Negative (LN), Zero (Z), Least Positive LP), and Most Positive (MP)

$$w_k = \mu_{Ai}(E).\mu_{Bi}(\Delta E) \tag{11}$$

Where w_k is the output of layer 2.

$$v_k = \frac{w_k}{w_1+w_2+w_3+\cdots w_{25}} \tag{12}$$

The membership functions obtained for each input are given below:

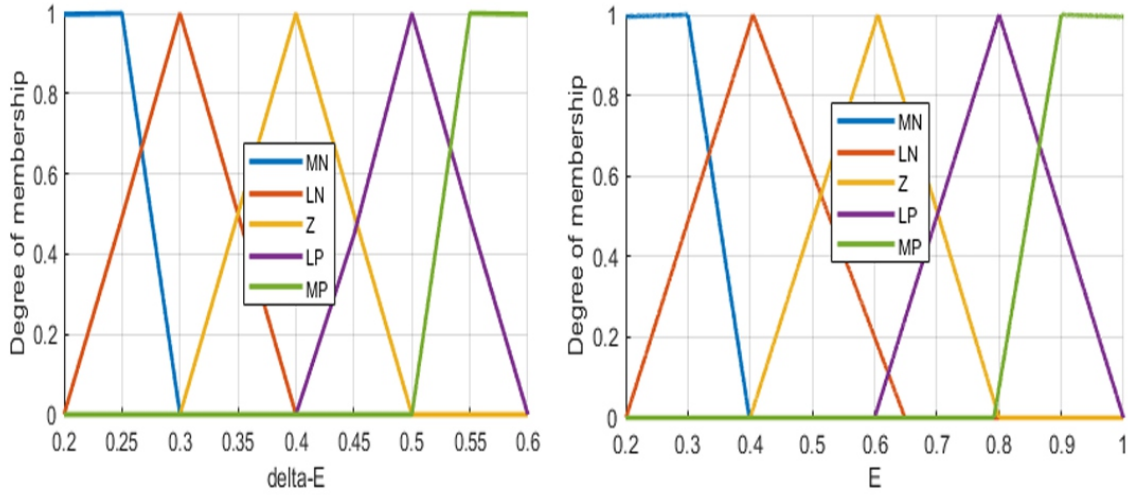

Figure 6. Membership functions of the inputs obtained.

$$o_k^4 = v_k . f_k = v_k(a_k . E + b_k . \Delta E + m_k) \quad (13)$$

Where v_k is the output of layer 3, and (a_k, b_k, m_k) is the set of output parameters of rule k.

The last layer is obtained by:

$$o_k^5 = \sum_{k=1}^{4} o_k^4 . v_k \quad (14)$$

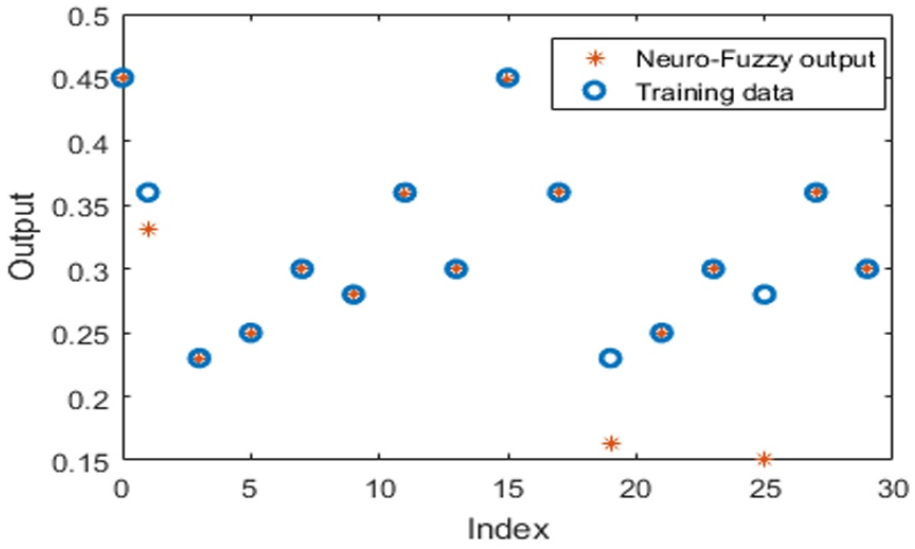

Figure 7. Training of the neuro-fuzzy network.

2.2.2. Determination of offset gains by the PSO

Particle swarm optimization (PSO) is an evolutionary computation technique developed by Eberhart and Kennedy (1995). This algorithm is inspired from the social behavior of animals, such as the flocking of birds and the schooling of fish, and the swarm theory. It has been proven to be efficient in solving optimization problem especially for nonlinearity and non-differentiability, multiple optimum and high dimensionality [35-38]. The many applications of this algorithm in several fields and particularly in the field of technology shows its superiority compared with other stochastic methods such as the genetic algorithm, biogeography, and the colony of the ants [38]. It is an algorithm itératif. À each stage of calculation which the values of the individuals are compared according to the function objectifies to place the new guides then are select. During its execution, the algorithm passes by the stages grouped in the following flow chart: The position and velocity of each particle are updated by applying the following equations:

$$V_{i+1} = w.V_i + c_1.r_1.(x_{ip} - x_i) + c_2.r_2.(x_g - x_i) \quad (15)$$

$$x_{i+1} = x_i + V_{i+1} \quad (16)$$

With:

$$w = w_{max} - iter.(w_{max} - w_{min})/iter\_max \quad (17)$$

x_{ip} and x_g respectively the best position of a particle i since the first iteration, and the best overall position of the swarm;

c_1 and c_2 are acceleration coefficients with a typical value of 2;

r_1 and r_2 are random numbers within [0, 1];

�� is the coefficient of the inertia weight, iter is the present iteration number, max and min subtitles stand for maximum and minimum, respectively. In addition, “iter_max” have been selected such that the best fitness function with a suitable convergence capability can be achieved. This value is 1000 in the simulation. Supporting the above mentioned PSO technique, the procedure of the PSO can be described by the flowchart shown in Figure 8.

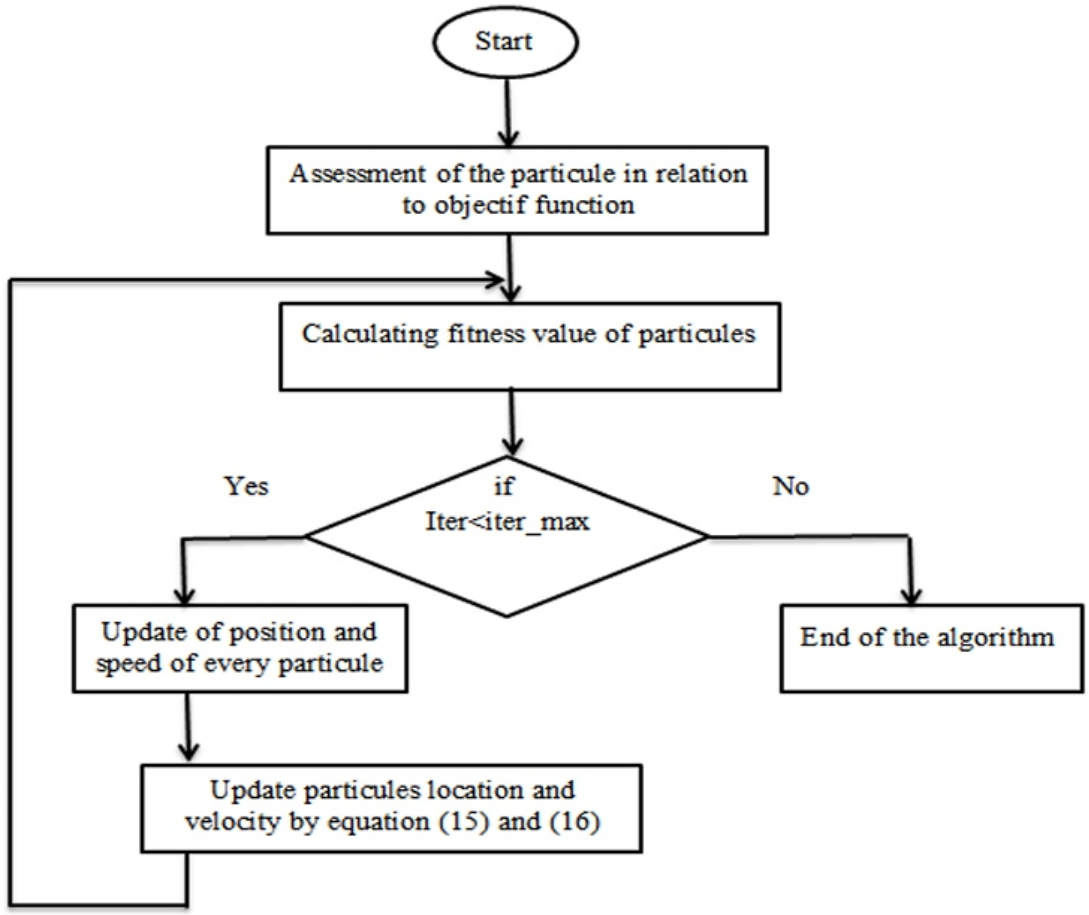

Figure 8. Flow chart of PSO algorithm

After realizing all the components of our method, we obtain the synoptic diagram of our method is presented in figure 9. We have combined Neuro-Fuzzy and PSO. Neuro-fuzzy is a hybrid artificial intelligence system that combines fuzzy logic and a learning algorithm derived from neural networks to determine the parameters of fuzzy sets and fuzzy rules from data; it is used because it can automatically generate the fuzzy rules. The PSO is a meta-heuristic; it is used here to determine the normalization gains, allowing to convert the real input values into fuzzy quantities, to readjust the dynamics of the fuzzy rules.

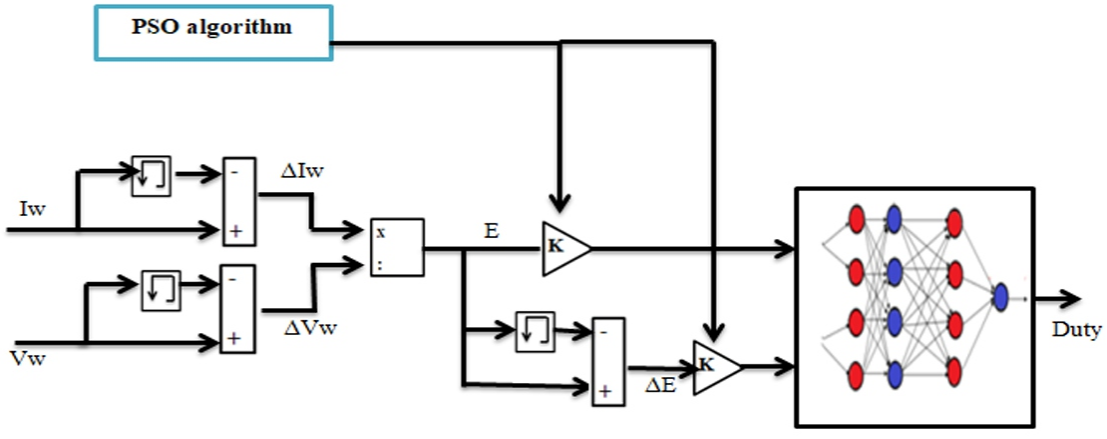

Figure 9. Design process of the hybrid method of MPPT developed

3. Results and discussion

In order to test the performance of the NF PSO MPPT controller, we performed several simulation cases. To verify the theoretical study on the behavior of the MPPT controller a series of imulationswas performed with Matlab/Simulink software and a comparison was made with the MPPT, NF and Cuckoo algorithm controllers

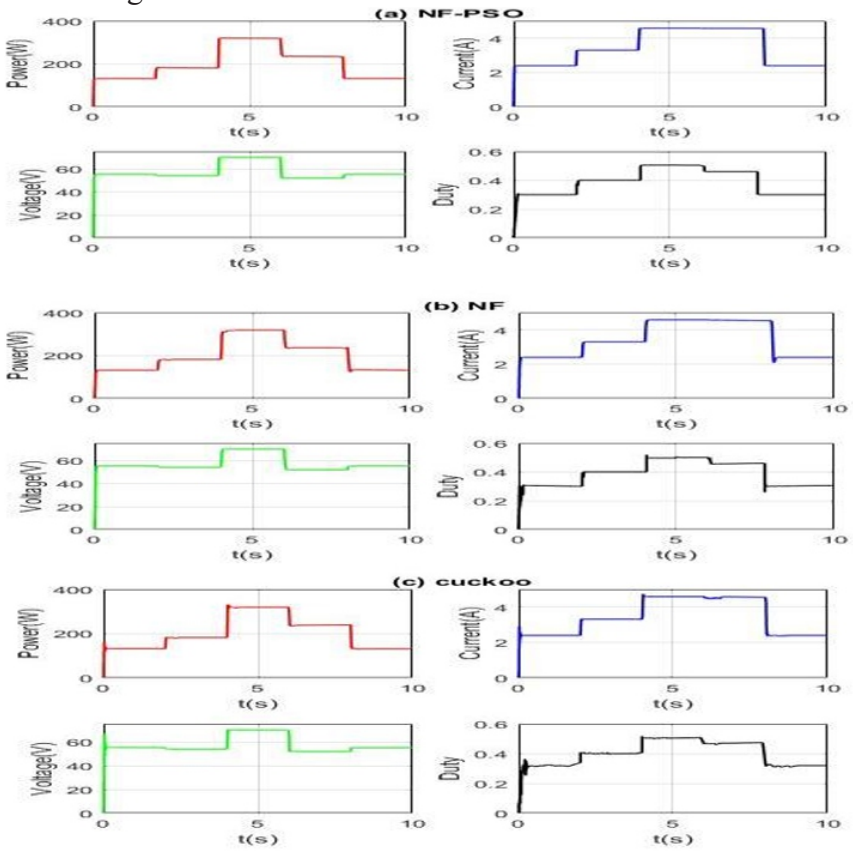

Figure 10. Curves obtained with different shading pattern variations using (a) NF-PSO, (b) NF, and © Cuckoo.

The simulation results in Figure 10 show the waveforms of power (red color), voltage (green color), current (blue color), and duty cycle (black color) obtained with the different methods. The results in Figure 10 confirm that the values of Ppv, Ipv, and Vpv reached the same values as those presented by the PV specifications in Table 1 and 2. To clearly see the effectiveness of our proposed MPPT method, we performed a co-simulation in Figure11.

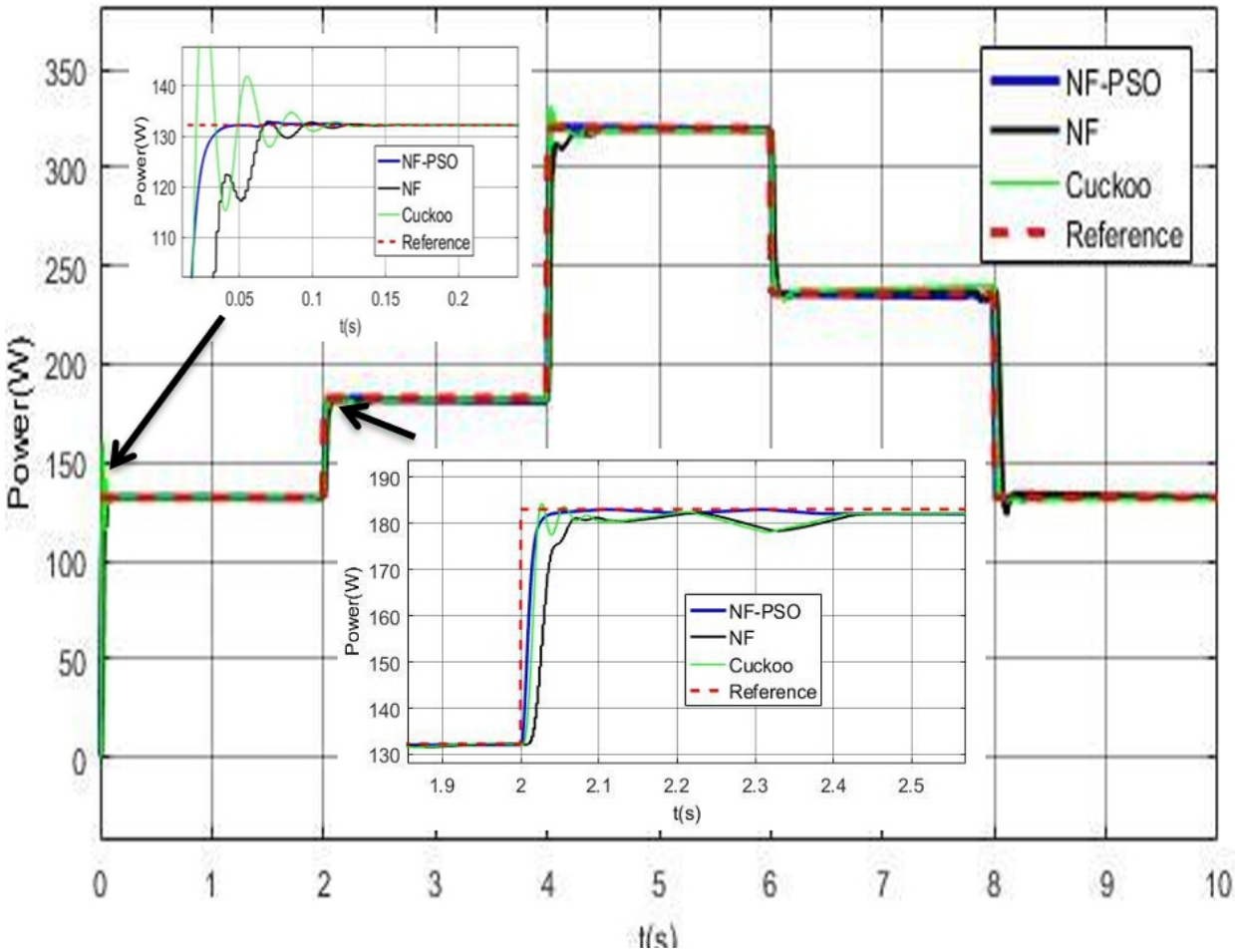

Figure 11. Co-simulation of the powers obtained with the different MPPT methods

For clarity, the performance of each method is summarized in Table 4. Although the numbers are not absolute, i.e.,given in ranges, they can be considered reasonable indicators of the relative performance of these methods.

Table 4. Comparison of the different MPPT methods

Algorithm	Tracking efficiency (%)	Response time (s)	Steady state oscillation (%/W)
NF-PSO	99.94	0.044	0.0009
NF	98.90	0.138	0.0404
Cuckoo	98.96	0.155	0.041

We notice that for the initial power rise from zero to steady state, NF-PSO seems to be the fastest; In addition, Cuckoo shows larger fluctuations in the transient regime; in terms of tracking accuracy, our method is more efficient with 99.94% and a response time of 0.0009s.

4. Conclusion

In order to improve the efficiency of partially shaded PV systems, especially their energy production, we have developed an intelligent and simple method based on NF and PSO. This strategy allows to optimize at each moment the maximum power available in a PV array operating under partial shading. Thus we started with the presentation of the used equipment. Then we presented the NF-PSO controller. The simulation results under different scenarios of partial shading show the advantage of the adopted strategy because it is faster with a response time of 0.044s, more efficient with 99.94%, also allows the reduction of oscillation with a rate of oscillation of 0.0009 %/W. In our future work we will make a comparative study by optimizing the Neuro-Fuzzy with two other iterative algorithms among which: Grey Wolf Optimization (NF-GWO), Whale Optimization Algorithm (NF-WOA) and compare with Particle Swarm Optimization (NF-PSO).

5. Acknowledgements

The authors would like to thank the journal editor and all organizations that provided data for this research.

Nomenclature

n: Ideality factor of the PN junction

K= 1.3805 × 10-23 [J/K]: Boltzmann's constant

q = 1.6 × 10^{-19} [C]: Charge of the electrons

T[K]: Temperature of the cell

Eg = 1.12 [eV]: Band gap energy of the semiconductor used in the PV cell

Io: Inverse saturation current

Iph [A]: Photo-current

Ior: Inverse saturation current at Tr

Ipv[A]: Current of the PV module

Vpv[V]: Voltage of the PV module

Ppv[W]: Power of the PV module

Iscr [A]: Cell's short-circuit current at the reference irradiation and temperature

Np: Number of cells connected in parallel

Ns: Number of cells connected in series

Tr [K]: Reference temperature of the cell

Voc [V]: Open-circuit voltage

D: duty cycle

x_{ip} : Best position of the particle at iteration i

x_i : Position of the particle at iteration i

x_g : Best position of its neighborhood at iteration i

c_1 and c_2: Acceleration coefficients

r_1 and r_2: random numbers within [0, 1]

w : Coefficient of the mass of inertia

V_{i+1} and V_i: velocities of the particle at iteration i and i+1

μ_{xi} : Membership functions of the linguistic terms x_i

μ_{yi} : Membership functions of the linguistic terms y_i

References

[1] Krishna, K..S. and Kumar, K..S. (2015). A review on hybrid energy systems. Renewable and Sustainable Energy,Reviews, 52, 907 – 916.

[2] Jubaer A. and Zainal S.A. (2014). Maximum Power Point Tracking (MPPT) for PV system using Cuckoo Search with partial shading capability. Applied Energy, 119, 118–130.

[3] Trihah E. and Patrick Chapman L. (2007). Comparison of Photovoltaic Array Maximum Power Point Tracking Techniques. IEEE trans. Energy Convers, 22, 439–449.

[4] Loubna B., Mohammed H., Bekkay H. and Hicham B. A (2017). New MPPT-based ANN for

photovoltaic system under partial shading conditions. Energy Procedia , 111, 924 – 933.

[5] Cyrus M. and Fazel M. (2019). Design and Analysis of a Stand-Alone Photovoltaic System for Footbridge Lighting. Journal of Solar Energy Research Spring, 4(2), 85-91.

[6] Smail C., Saad M., Aboubakr El H., Aissa C., Abou S.B., Abdelaziz E.G., Aziz Derouich, Mohamed A. and Askar S. S. (2022). A novel hybrid GWO–PSO-based maximum power point tracking for photovoltaic systems operating under partial shading conditions. Scientifc Reports, 12:10637.https://doi.org/10.1038/s41598-022 14733-6

[7] Makhloufi S. and Mekhilef S. (2022). Logarithmic PSO-based global/local maximum power point tracker for partially shaded photovoltaic systems. IEEE Trans. Emerg. Sel. Top. Power Electron,, 10. 1. 375–386.

[8] Ibrahim S., Pei C.C., Dawit F.T., Ramadhani K.S., Kuo L.L., And Jia-Fu L. (2022). An Enhanced Grey Wolf Optimization Algorithm for Photovoltaic Maximum Power Point Tracking Control Under Partial Shading Conditions. Industrial Electronics Society, 3, 392-408.

[9] Ma X., Jiandong D., Xiao W., Tuo C., Yanhang W., and Ting C. (2018). Research of photovoltaic systems MPPT based on im proved grey wolf algorithm under partial shading conditions. in Proc. 2nd IEEE Conf. Energy Internet Energy Syst. Integration, DOI: 10.1109/EI2.2018.8582098, 1–6.

[10] Guo K., Cui L., Mao M., Zhou L., and Zhang Q. (2020). An improved gray wolf optimizer MPPT algorithm for PV system with BFBIC converter under partial shading. IEEE Access, 8, 103476103490.

[11] Eltamaly A. M. and Farh H. M. H. (2019). Dynamic global maximum power point tracking of the PV systems under variant partial shading using hybrid GWO-FLC. Sol. Energy, 177. 306–316.

[12] Femia N., Petrone G., Spagnuolo G., and Vitelli M. (2005). Optimization of Perturb and Observe Maximum Power Point Tracking Method. IEEE Trans. Aerospace .Electro systems, 20. 4. 963–973.

[13] Safari A. and Mekhilef S. (2011). Simulation and Hardware Implementation of Incremental Conductance MPPT With Direct Control Method Using Cuk Converter. IEEE Trans. Indus. Electron, 58(4), 1154–1161.

[14] Premkumar M., Umashankar S., Thanikanti S., Sanjevikumar P., Jens B., Mssimo M., and Sowmya R. (2021). Improved perturb observation maximum power point tracking technique for solar photovoltaic power generation systems. IEEE Syst. J., 15(2), 3024–3035.

[15] Bayata P. and Baghramian A. (2019). A High Efficiency On-board Charger for Solar Powered Electric Vehicles Using a Novel Dual-output DCDC Converter. Journal of Solar Energy Research, Spring, 4(2), 128-141.

[16] Kitmo, Guy B. T., Dieudonné K. K., Sadam A., and Noël D. (2021). Optimization of the Smart Grids Connected using an Improved P&O MPPT Algorithm and Parallel Active Filters. Journal of

Solar Energy Research, Summer 6(3), 814-828.

[17] Claude Bertin N., Fapi, Martin Kamta, and Patrice Wira. (2019). A comprehensive assessment of MPPT algorithms to optimal power extraction of a PV panel. Journal of Solar Energy Research, Summer 4(3), 172-179.

[18] Killi M. and Samanta S. (2015). Modified perturb and observe MPPT algorithm for drift avoidance in photovoltaic systems. IEEE Trans. Ind. Electron, 62(9), 5549–5559.

[19] Alajmi B. N., Ahmed K. H., Finney S. J., and Williams B. W. (2011). Fuzzy-logic-control approach of a modified hill-climbing method for maximum power point in microgrid standalone photovoltaic system. IEEE Trans. Power Electron., 26(4), 1022–1030.

[20] Tey K. S. and Mekhilef S. (2014). Modified incremental conductance algorithm for photovoltaic system under partial shading conditions and load variation. IEEE Trans. Ind. Electron., 61(10), 5384–5392.

[21] Özgür C. and Ahmet T. (2017). A Hybrid MPPT method for grid connected photovoltaic systems under rapidly changing atmospheric conditions. Electric Power Systems Research, 152, 194–210.

[22] Alireza. R, Ali. E, Hasan. E and Mohammad. M. (2017). Intelligent hybrid power generation system using new hybrid fuzzy-neural for photovoltaic system and RBFNSM for Wind turbine in the grid connected mode. Front. Energy, DOI: 10.1007/s11708-017-0446-x.

[23] Alireza Z., Iman S., and Bahador F., (2021). A Partial Shading Detection Algorithm for Photovoltaic Generation Systems. Journal of Solar Energy Research, Winter 6(1), 678-687.

[24] Ahmad. R, Hossein. K. and Mahdi. M. (2013). A Comprehensive Method for Optimum Sizing of Hybrid Energy Systems using Intelligence Evolutionary Algorithms. Indian Journal of Science and Technology, 6 (6), 0974-6846.

[25] Shams I., Mekhilef S., and Tey K. S. (2021). Maximum power point tracking using modified butterfly optimization algorithm for partial shading, uniform shading, and fast varying load conditions. IEEE Trans. Power Electron., 36(5), 5569–5581.

[26] Raeisi H. A. and Sadeghzadeh S. M. (2019). Designing and Construction of a Solar Panel Simulator Capable of simulating partial shading conditions. Journal of Solar Energy Research, 4(1), 15-21.

[27] Mazaheri Salehi P. and Solyali D. (2018). A review on maximum power point tracker methods and their applications. Journal of Solar Energy Research, 3(2), 123-133.

[28] Venkateswari R., and Sreejith S. (2019). Factors influencing the efficiency of photovoltaic system. Renewable and Sustainable Energy Reviews, 101, 376–394

[29] Oulcaid M., El Fadil H., Yaliya A., and Giri F. (2016). Maximum power point tracking algorithm for photovoltaic systems under partial shaded conditions. IFAC-paperOnline, 49(13), 217-222.

[30] Syafaruddin Karatepe E., Hiyama T. (2009). Artificial neural network-polar coordinated fuzzy controller based maximum power point tracking control under partially shaded conditions. IET Renew Power Gener, 3, 239–53.

[31] Mostefa K. and El Madjid. B. (2017). Artificial intelligence-based maximum power point

tracking controllers for Photovoltaic systems: Comparative study. Renewable and Sustainable Energy Reviews, 69. 369–386.

[32] Premkumar M. and Sowmya R. (2019). An effective maximum power point tracker for partially shaded solar photovoltaic systems. Energy Reports, 5, 1445–1462.

[33] Jyh-Shing Roger Jang. (1993). ANFIS: Adaptive-Network-Based Fuzzy Inference System. IEEE Transactions on systems, Man, and Cybernetics, 23(3), 665-685.

[34] Vlachos D. and Tolias Y. A. (2003). NeuroFuzzy modeling in bankruptcy prediction. Yugoslav Journal of operations Research, 2, 165174.

[35] Chiou, J.S. and Liu, M.T. (2009). Numerical simulation for Fuzzy-PID controllers and helping EP Reproduction with PSO hybrid algorithm, Simulation. Modelling Practice and Theory, 17, 1555–1565.

[36] Bouarroudj, N., Boukhetala, D. and Boudjema, F. (2014). Tuning Fuzzy PDα sliding mode controller using PSO algorithm for trajectory tracking of a chaotic system. Journal of Electrical Engineering, 14(2), 378–385.

[37] Bouarroudj, N., Boukhetala, D. and Boudjema, F. (2015). A hybrid fuzzy fractional order PID Sliding-Mode controller design using PSO algorithm for interconnected Nonlinear Systems. Journal of Control Engineering and Applied Informatics, 17(1), 41–51.

[38] Abdelhalim B., Noureddine B., Abdelhak B. and Layachi Z. (2017). P&O-PI and fuzzy-PI MPPT Controllers and their time domain optimization using PSO and GA for grid-connected photovoltaic system: a comparative study.

ISSN. 2476-1234

Feasibility Construction of a 4 MW PV Power Plant to Provide Sustainable Electricity to Bandar Abbas Industrial Estate

Majid Zarezadeha a

Iranian National Standard Organization, Administraion Standard of Hormozgan, Bandar Abbas, Iran

A B S T R A C T

The upward increases in electricity consumption in the last decade and excessive use of electricity in these years have challenged the electricity industry and related industries. The blackout caused by this increase in consumption leads to losses for manufacturing companies and workshops. The location of Hormozgan province has created this mentality for researchers that due to high humidity and dust, it is not possible to use PV power plants. The possibility of installing a 4 MW PV power plant in Industrial Estate No 2, has been investigated, and the simulation results with PVSol, PVSyst, and RETScreen software have shown that the location is a suitable place to install the power plant, and there is a possibility of obtaining suitable energy and supporting the industrial estate. In the selected position, it is possible to get suitable solar energy for more than eight months of the year, and solar energy could be used for more than 10 hours a day. The output of the simulations also showed that the construction of the PV power plant in this location with a performance factor of 0.7 and an average output power of 3.2 MW would be good efficiency. Since the hours of solar energy production correspond to the electricity peak hours of consumption, the PV power plant can be used as a suitable alternative for producing stable electricity and preventing power outages during peak hours of production units and factories. The use and comparison between south-facing panels and delta wing and the use of these types of equipment in the hot and humid climatic conditions of Hormozgan province have been done for the first time in this research.

Keywords: *Computer Simulation, PVSol, PVSyst, Renewable Power Plant, Solar Energy, Sustainable Electricity*

1. Introduction

Considering that energy is one of the determining indicators in economic development, the development and optimization of renewable energy can play an effective role in economic growth and protection of environmental conditions. They point to the policies that ultimately determine the priority and necessity of using some of them for the country and explain why and how to use them. Using solar energy to supply hot water to homes and industrial centers is one of the most cost-effective ways to use solar energy in oil-burning villages in Iran. For scattered users far from the grid who need relatively little power, photovoltaic is almost a competitive or low-cost technology. Photovoltaic has a strong and modular structure and requires little maintenance, and is, so, very suitable for remote rural users. For older users, it seems best to hybridize with wind or fossil fuels [1]. The importance of electricity in the production and economy of Iran comes from the fact that the electricity industry has a high value in the national economy and provides economic and social welfare to countries, and is one of several great

infrastructure industries. Especially in industries, electricity has a particular grade because, in most cases, electricity drives the machinery of factories and makes all operations and production activities possible, and for this reason, some experts have considered the electricity industry as the mother of industries. The optimum time for a preventive replacement of renewable energy devices varies from one geographical location to another because each geographical location has its climatic fluctuations. The higher the occurrence of climatic fluctuations in a geographical location, the shorter the optimal time for preventive replacement of the device. The higher the average occurrence of climatic fluctuations, and as a result, the greater the optimal time for the protective replacement of the device. It was also indicated that the better the industrial qualifications (that is, a greater tolerance limit for the device), the greater the optimal time for a preventive replacement for the device. Therefore, companies that export these devices must study the geographical location where the device is exported and the climate in which it is distinguished to develop plans and programs to protect the device [2]. One of the major challenges faced in photovoltaic technology is the ability to harvest as much energy as possible from the sun. The peculiarity in geographic location and the sun's movement has made it hard to get maximum irradiation from the sun. [3].

Based on research by Khazaee et al, most Asian countries have the capacity for renewable energy, including solar, hydro, wind, etc. Asian countries are geographically placed in an area with various climatic circumstances including tropical, and humid. Hence, easy access is provided to various renewable energy sources. Studying the years 2000 to 2019 comprehensively, the results revealed that China, India, and Japan had the most renewable energy capacity in Asia with 790000 MW, 133000 MW, and 120000 MW in 2019 respectively. Also, the energy produced by renewable energy for these countries in 2019 was 1739400 GWH, 288622 GWH, and 190587 GWH respectively [4]. The use of renewable energy in residential buildings has main environmental and social effects. Noorollahi et al researched energy consumption in buildings. According to this research, 89% of thermal demand in the building section of Iran is supplied by natural gas, but it can be used more in the current industrial infrastructure if renewable resources supply buildings' thermal demand. Different scenarios were discussed for this research by considering the amounts of CO2 emission and total energy cost. The results showed all procedures led to CO2 emissions reduction due to reducing natural gas consumption. Based on the results, using solar thermal collectors decreased the average total cost by about 13%. In conclusion, considering the current national natural gas distribution network in Iran, using solar thermal collectors was the best alternative solution [5]. Reducing greenhouse gas (GHG) emissions-induced environmental hazards is one of the most important goals of future research on the energy economy and the environment. This study aims of Pourarshad et al, to visualize emissions from electricity generation in Khuzestan province, southern Iran. Khuzestan's electricity supply and demand

system was simulated and examined under green scenarios till 2050 by assessing the existing situation and choosing a suitable low-carbon energy system for the future. One of the results of this research is to reduce emissions in terms of energy management strategies in the short term and the ineffectiveness of development strategies regardless of consumption management strategies. Electricity supply optimization scenarios are attractive in the long term, which indicates the costly implementation of development strategies. Combining solutions to balance the energy economy and environment is more effective. The OKEP scenario as a combination of consumption management and development strategies showed that it would maintain its positive impact in the short and long term and successfully reduce emissions. In this scenario, the net present value (NPV) attractiveness is over $ 6706 million and saves the emission of 179 MtCO2e. Compared to the business as usual (BAU) scenario, more than 90 Bm3NGe savings and a 3.62% increase in renewables share are other benefits of this scenario [6]. Similar research was also done in Poland on the effect of building and using photovoltaic renewable power plants on the reduction of harmful gas production by Lew et al. Poland is one of the European leaders in photovoltaic development, and according to estimates for 2021–2025, it will continue to be. The results obtained from the survey allowed us to draw conclusions, which include the following: (1) a lack of general conviction of respondents about the effectiveness of Poland's decarbonization policy on reducing global CO2 emissions, especially among those who show a higher willingness to use PV installations, (2) the willingness to use PV installations is motivated by rather than environmental benefits, (3) the need for more widespread public campaigns aimed at promoting the benefits of decarbonization and renewable energy sources, and (4) the finding that the respondent's region of residence (with a different degree of insolation) mattered for the willingness to use PV installations [7].

Also, in another research in Turkey and a climate similar to the climate of southern Iran with high humidity, the variable albedo effects on bi-facial PVs in different ground conditions were examined. The results were compared with monofacial PV panels in the same conditions for the Konya region. Bifacial PV panels were analyzed under white, sand, and asphalt ground conditions. Simulations were made by the PVsyst program, and the results were compared by global radiation value, the performance ratio (PR), and the produced energy results. An capacity of 54,6 kWp bifacial and monofacial installed PV panels with a horizontal angle of 35°, azimuth angle of 0°, and 6m intervals for roof installation is considered [8].

Climatic conditions are a very effective factor in the construction of photovoltaic power plants. according to this in colombia, Narvaez and et al present the first study of the long-term climatechange impact on photovoltaic power potential in Nariño, Colombia. Their results suggest that changes in photovoltaic power potential, by the end of the century, will have a maximum decrease of around

2.49% in the central zone of Nariño, with some non-affected areas, and a maximum increase of 2.52% on the south eastern side with respect to the pessimistic climate change scenario [9]. Ibrahim and et al monitor the trend of extreme temperature and analyze its impact on solar power plants in Malaysia. The basic energy parameters of the solar photovoltaic module are calculated to find out the relationship between ambient temperature and power generated. It is found that the output power of the solar photovoltaic module is reduced about 0.3 to 0.5 % for every 1 °C ambient temperature increases [10]. Although research in hot and dry climates has shown that a portion of this power can be used to cool solar panels through various means to keep their efficiency high, such as running air fans or running pumps to cool them with coolant [11].

In new research Considering Iran's potential in the field of solar energy and the country's need for this type of energy, it is necessary to locate and identify suitable sites for the use of solar energy. In this research, the potential of generating power from solar energy on the ocean coasts of south-eastern Iran has been investigated. The geographical data of the solar radiation map of Iran was used to estimate the power of electrical energy from spatial limiting criteria for the feasibility of installing photovoltaic panels at the power plant scale. The total power of electricity that can be extracted from suitable places in the region was calculated, which shows the high potential of the south-eastern coast of Iran in benefiting from renewable energy, which can be a driving force for the industrial, economic, and social development of the Makran region. Calculations show that only with the construction of photovoltaic power plants with a total capacity of 3,000 megawatts in the study area, which covers only about half a percent of very good land, the total electricity generated by the current power plants in Sistan and Baluchestan can be replaced the year 2016. This is a good indication of the high potential of solar energy in the Makran region, which has been neglected so far [12]. In similar studies with the southern climate of Iran, acceptable results have been obtained from the use of renewable solar energy. In the analysis for Chandigarh in India, a 100-kW photovoltaic plant is analyzed for the selected area with different PV panel combinations for finding the optimal solution for power generation. This selected area is having a good solar radiation reception potential of 5.07 kWh/m2/day annually at an annual 25.4oC temperature. The plant is designed with fixed axis orientation and has a tilt of 31o. The plant has the potential to export 156120 kWh of electricity to the grid with a performance ratio of 76% [13].

The importance of using solar energy in the Persian Gulf countries is well understood. Despite the existence of abundant oil and gas resources, the countries of the Persian Gulf have made appropriate investments in this area and have long-term plans. Now all GCC countries had conducted, relatively, large project in solar and wind energy, especially Kuwait (currently about 70MW among a plan of 2000MW by 2030), UAE (currently about 300MWamong a plan of 2500MWby 2030) and Saudi

Arabia (with an ambitious renewable energy target of 3450MW by 2020 with a further 6000GW envisioned by 2023 and to 200 000MW by 2030) [14].

The use of PV in setting up industries and workshops is increasing rapidly today. Kim and et al study, a comparative economic analysis was conducted for typical greenhouses, plant factories with natural and artificial light, and those with only artificial light, based on the insulation, artificial light, and photovoltaic (PV) installation costs. the case of the installed PV systems exhibited large reductions, of 424% and 340%, in terms of primary energyconsumption and GHG emissions, respectively [15]. Bangladesh has a considerable number of large manufacturing plants with appropriate roofs that could be used for deploying solar energy conversion systems at scale. Talut and et al, in Bangladesh presented which identified and assessed 6045 such plants, which have roof areas ranging from 100 m2 to 50,000 m2, and modelled the deployment of solar photovoltaic (PV) technology that can provide power through site available grid infrastructure. The results showed that around 7.4 GWp of PV capacity can be achieved on such roofs with a corresponding annual electricity generation of 11 TWh [16]. Desai and et al To overcome the problem of continuous grid supply of electricity and diesel generator sets, solar based refrigeration system for milk cooling at society level is quiet feasible. The results showed Use of solar energy has great scope for its commercial use in the dairy processing operations as well as to design and develop solar based refrigeration systems for dairy industry [17]. Solar energy has also been used to run mining equipment. The copper mineral processing industry faces complex scenarios with increased demand, highly variable energy prices, falling ore grades that increase energy consumption, and increasing concern about the industry's carbon footprint. To reduce the risk imposed by these scenarios, the industry is looking at the use of renewable energy sources. Behar and et al investegated use of solar thermal and solar photovoltaic technologies to produce power and heat for the copper mining processes. Results showed the use of solar energy in the copper mineral processing industry could solve present energy-related problems particularly GHG emissions. To fully utilize the solar potential, toward all-solar-powered mining industry in Chile, innovative and cost-optimized processes and operations should be introduced [18]. Farjana and et al, investigated this issue in lead mines. Comparative analysis among seven miner countries is conducted by considering a few cases based on solar industrial process heating system design. The analysis results showed that buffer tank system with solar loop heat exchanger but without flow heater would be the most beneficial in terms of solar fraction, emission reduction, and annual fuel savings. These results showed that evacuated tube collector installation in the industrial processes would be the most beneficial irrespective of the cost of solar energy [19]. Site selection to build a renewable solar power plant and going through this process helps to optimize the final result and reduce costs. Researchers and scientists in institutes and research centers around the world mainly used a combination of AHP, WLC, and IDW methods in a GIS

environment[20-24].

The geographical location and weather conditions of Hormozgan province, in the south of Iran, are such that the supply of sustainable water and electricity for domestic, agricultural, commercial, and production purposes have been one of the constant challenges for the managers of Hormozgan province. Every year, especially in recent years, as the hot season begins, the concern about the lack of electricity, followed by widespread blackouts throughout the country, is intensified. This issue has become an important challenge, especially in the first six months of every year, when the temperature rises rapidly, the annual decisions in this matter mainly push the priority of consumption to the home consumers. It causes scheduled or unplanned interruptions for industries and makes their production difficult. Based on the specific conditions of production costs, the price of subscribers increases by 20% in the summer. The problem of not providing stable electricity in industries, in addition to creating costs on production and the final product, will lead to a delay in delivering products to customers and as a result losing a part of the market.

Due to the noticeable increase in temperature in the first six months of the year in Hormozgan province, the conditions for using electricity for government executive bodies, organizations, and industries have become stricter and are subject to blackouts, most of which are during peak consumption hours, it is from 13:00 to 17:00. The great heavy industries of Hormozgan province, especially in the metal field, are located in the west of Bandar Abbas city and the special economic zone of the Persian Gulf, mining and metal industries, which use very high energy due to their type of work. Other industries, and workshops are in 15 industrial estates. Seven industrial areas are located throughout the province. One of the ways to use stable and separate electricity from the national grid for production units in these industrial estates is to use renewable energy, especially solar energy. Due to the view that the climate of the province has high humidity and dusty conditions, the use of solar energy in Hormozgan province is not wellunderstood, but the results of different research have shown that solar cells in tropical regions also have an acceptable performance [25]. Many people's idea of solar energy is focused on turning on traffic lights or weak electricity generation from it. Because they think that since electricity is produced by sunlight, it cannot have enough power to supply large power. It is possible to produce up to megawatts of electricity through solar panels, and make it ready to be used for various purposes or to contribute to national electricity. Supplying three-phase electricity through solar energy or battery banks can be a solution for many industries that are either unable to supply electricity from the national grid or their required power exceeds the maximum power of the grid. In this research, as a pilot, the possibility of generating electricity from a solar power plant near Bandar Abbas Industrial Estate No 2 has been investigated, and its results have been presented.

2. Materials and Methods

The method used in this research started with the preliminary study of similar articles and experiences in the energy field. Considering that energy is needed for industries and workshops, based on that, the land required for the power plant needed and the amount of consumption have been determined. The climatic conditions and weather of the region as well as the radiation in the region have been investigated. These data are taken from meteorological databases, articles as well as international online databases. Based on the relevant standards and technical and legal requirements, a suitable place for the construction of the photovoltaic power plant has been located. After determining the amount of electricity consumed, the site selection for the construction and simulation of the solar power plant has been determined. This location is based on technical requirements using the site selection feature in ArcGis software. The capability of this software and entering appropriate data to choose the location is the appropriate capability of this software. After determining the required energy consumption and suitable location, a simulation has been done using the software. Finally, the effects and environmental results of the construction of this photovoltaic power plant have been calculated by the RETScreen software. Since the analysis of statistical results is important, the results have been analyzed using the hypothesis test using the Minitab software.

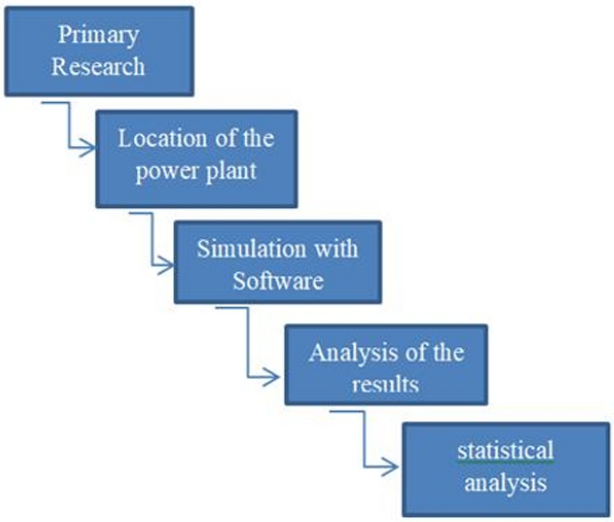

Figure 1. Schematic of the research method

2.1. ESTIMATING THE AMOUNT OF ELECTRICITY CONSUMPTION IN THE PILOT LOCATION

Bandar Abbas Industrial Estate No 2 is located on an area of about 70 hectares, 20 km from Bandar Abbas city and in the position 27.20 N longitude and 56.20 E latitude in the north of this city (Figure 2). This industrial estate has 20 factory units and workshops. Of these 11 units are generally working permanently and other workshops and units are seasonal and temporary. According to the statistics obtained from the Hormozgan Electrical Company as well as the industrial settlements company, according to the size of the area, the electricity requirement of this place to run the units and provide lighting and other related services is on average about 3 MW. Of course, the amount of consumption is higher in the hot seasons of the year, and the main challenge is to provide stable electricity in these seasons.

Figure 2. The location of the industrial Estate and surrounding lands

2.2. DETERMINIG THE INSTALLATION LOCATION OF PV POWER PLANT

To construct a PV power plant, two plots of flat area in the east of the industrial estate with an area of 5

hectares and west of it with an area of 10 hectares were considered and selected to investigate other effective factors. The weather information of the region obtained from international climatological authorities shows that the proposed location has suitable conditions for temperature, radiation, pollution, and reflection coefficient throughout the year (Table 1) [26,27].

Table 1. Environmental conditions of the study area

	GolbHor KWh/m^2	DiffHor KWh/m^2	T_amb °C	Globinc KWh/m^2	GlobEff kWh/m^2
January	125.5	35.9	17.23	183.6	172.4
February	122.4	56.5	19.41	153.5	142.1
March	157.7	80.1	23.05	175.4	160.4
April	183.1	85.0	27.28	184.8	170.3
May	215.5	92.1	31.97	199.3	184.2
June	216.1	97.5	33.81	192.3	177.5
July	207.7	102.6	34.92	188.8	174.2
August	191.8	99.5	34.36	186.7	172.3
September	172.9	74.4	32.14	186.7	171.8
October	160.3	56.0	29.73	198.7	183.0
November	128.3	37.9	23.64	179.6	169.1
December	115.4	35.0	19.00	172.7	162.6
Year	1996.6	825.3	27.26	2202.2	2039.8

The study and field visit of two pieces of land, east, and west, near the industrial estate, have almost the same topography conditions. Due to the absence of tall or low-rise buildings in the area, the shading effect on the installed panels due to the topography is zero. After estimating the soil samples, standard penetration test, triaxial resistance, direct cutting, hydrometry, and granulation tests were performed on the samples [28, 29]. According to the results of the tests, the ground in this area is of hard soil type and therefore it has suitable conditions for installing the base structure of the panels and making them stable. The soil in the area will have the necessary strength, and in case of a strong storm, the pollution of soil and sand is low [25,30]. In terms of access to the industrial town as well as the national electricity network, the location of the western flat land has more suitable conditions, and therefore this land was chosen as a pilot site for the installation of equipment.

Figure 3. The open areas selected for the installation of the PV power plant in (a) east and (b) west of the industrial estate

Another point about this part of the selected lands is the lack of cultivation capability due to their soil type, and therefore, in terms of environmental permits, and government organizations, this place will not have any problems. Using ArcGIS software, the location of the land and its area has been calculated. After Geo referencing the plot of land, its exact location and topology status were examined .

Also, according to the topological map, the western land is far from the plain, and the probability of the area getting waterlogged due to seasonal rains is less than the eastern part [27,28]. In the final stage of determining the location of the power plant, the DEMa data of the area was collected. After that, this data is drawn by Global mapper software. The result of this data mining showed that the height of the area is higher than the surrounding areas. As a result, in case of rain or flood, this area will not be affected by them (Figure 4).

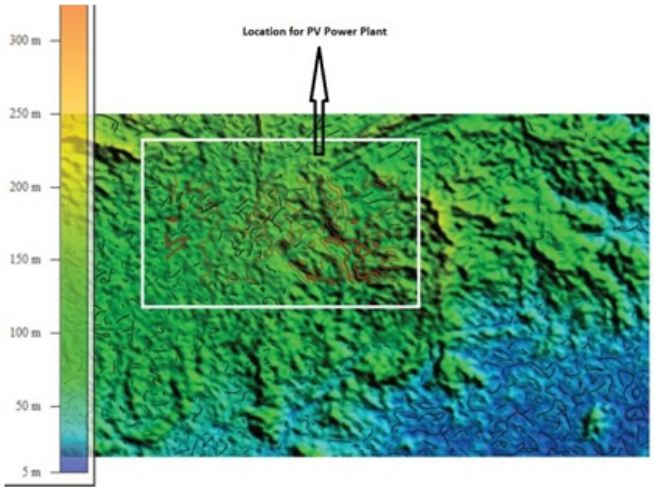

Figure 4. The topography of the west area location

2.3. CLIMATE AND SUN PATH OF LOCATION OF PV INSTALL

Examining the path of the sun from scientific and international sources [31], showed that the selected geographical location has a good conditions in terms of the time of effective radiation and the amount of radiation (Figure 5). Also, the amount of radiation and the environmental conditions of the installation location have a considerable amount of direct and return radiation (Figure 6).

According to climatological calculations, in terms of average solar energy, the location of Bandar Abbas Industrial estate No 2 has a good condition (Figure 6). The average amount of solar radiation energy is 1729.5 Kwh/m2. The clear sky and direct sunlight as a divine gift for Hormozgan province is a necessity to exploit in the production of cheap wealth in the form of setting up solar energy panels. Because, producing electricity with sunlight reduces people's costs. Between 340 and 350 days a year, Hormozgan province has the best capacity to use clean and pollution-free energy from the sun and produce electricity from this energy source, which is one of the unique capacities of this southern region in the country and even the world. The use of new and clean energies such as solar energy in provinces like Hormozgan, where 95% of the days of the year benefit from the blessing of sunlight, can also be an inspiring and income-generating event for people, especially those in need.

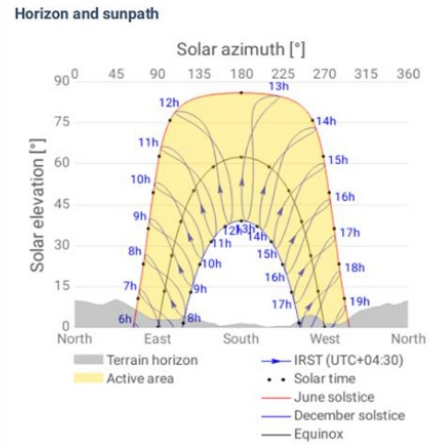

Figure 5. The sun path during the year in the desired position to install the equipment of PV power plant

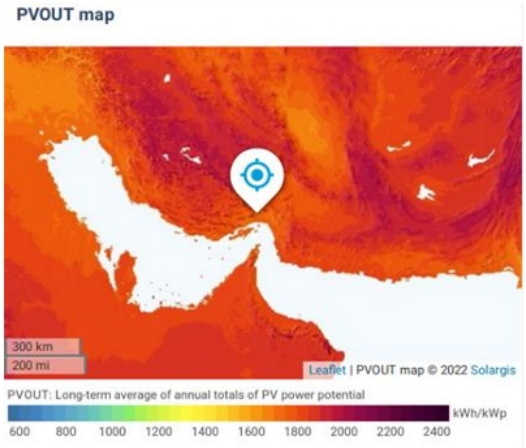

Figure 6. Average annual PV power potential in industrial estate location [31]

The windrose of Bandar Abbas station is shown in Figure 7. The prevailing wind in this station is south, then the south-southwest, north, and northnortheast directions have the highest frequency of the wind. The speed is greater than 12 m/s only in the south direction and with negligible frequency. In most directions, the wind speed is lower than 10 m/s. The northwest direction has the lowest frequency [32]. From the south to the northwest, the wind frequency has a decreasing trend, then it increases to the north, and after it has a decreasing trend to the east. In Figure 6, the monthly winds of Bandar Abbas station are presented for comparison. In this figure, it can be seen that the prevailing wind direction is south in all months except for December and January. In the two mentioned months, the prevailing wind direction is north since mid-winter.

Speed over 10 m/s starts from the south and continues until the beginning of autumn. The highest frequency in these months is related to the speed range. It is 6-10 m/s, which blows from the south. The western winds have weakened since the middle of spring and until the end of autumn, almost no wind blows to the Bandar Abbas area. The general trend of changes in the different speeds is almost the same in different seasons of the year. The difference is that the speed values decrease a little from early spring and increase a little from October onwards. Speeds over 4 m/s have a probability of 50% in different months [32].

In winter, systematic westerly winds, whose directions have become southwesterly winds following the coastline and the mountains aligned with it, and have been weakened by the effect of the mountains, in the daytime, combined with sea breezes, have created dominant southerly and southwesterly winds in Bandar Abbas. The north and northeast winds in this season are caused by the rule of the Siberian cold high-pressure system over this region and in this season, but these winds are weak during the day due to the direction opposite to the daily breeze and strengthen at night due to the alignment with the night breeze. As a result, what has appeared as the prevailing wind in this season in windrose is completely the land and sea breeze intensified by the mountains behind this region [33].

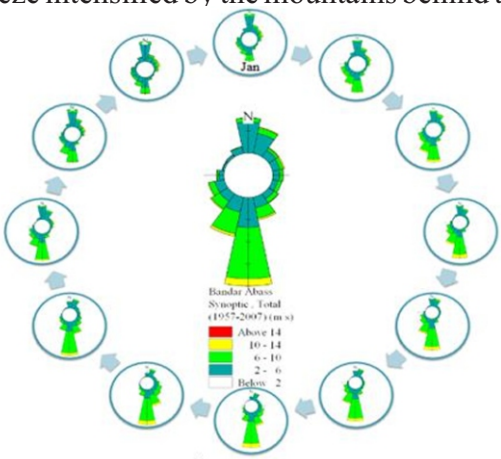

Figure 7. Average Monthly windrose Bandar Abbas from the synoptic station [30]

2.4. MODELING THROUGH SOFTWARE

After obtaining the initial field data and determining the appropriate location for installing the said power plant, PVsyst and PVsol software were used to simulate 4 MW PV. PVsol software has high power in 3D simulation and it is possible to obtain suitable output data from it. Also, to ensure the output results and data control, PVsyst software has been used. To simulate, 550 Watt panels were used in two rows and 50 panels in each row. To reduce the design costs, fixed angle panels, and 24 degrees angles were placed on the ground. The determined angle after monitoring the software and finding the optimal angle corresponding to the latitude of the installation location, which leads to the best output performance of the power plant, is selected and determined in the software input. To prevent the panels from shading each other and according to the height of the panels, the appropriate distance between the panels was determined using equation (1) of about 6 meters [29].

$$\beta_N = L - \delta \quad (1)$$

Where L is the Azimuth, is the δ height angle and β_N is the tilt angle of the sun to the latitude of the region. Hofmann algorithm is used for diffuse radiation [34]:

$$E_{clear} = 0.78E_{ext}\ \sin(\gamma_S)^{1.15} \quad (2)$$

Where γ_S elevation of the sun and Eext is the extra-terrestrial irradiation. The Hey&Davies algorithm for radiation equations on inclined surfaces. An anisotropy index, Ai, is defined is [35]:

$$A_i = \frac{DNI}{E_a} \quad (3)$$

Where DNI is the direct normal irradiance and Ea is extraterrestrial radiation.

Regarding the power of the panel, the inverter used to produce 4 MW power, both softwaressuggested the number of 8000 panels. The 3-phase electricity production and the power output of the power plant were estimated to be about 2.3 MW based on the simulation. To increase the efficiency of the process, the used panels are of single crystal type and have an efficiency of 21.29 and consist of 144 cells, a filling factor of 78.74%, and 50 KWinverters.

The advantage of Iran and especially the southern provinces is the existence of vast lands for building solar power plants, but it should be noted that the optimization of the area required for the installation of equipment, their control and monitoring will make it easier, and will lead to the reduction of other current costs. Based on the simulation, the amount of land required for this power plant is around 20000 square meters. This is the amount of area used in the case of fixed southfacing angle panels.

Due to the same initial conditions and the use of similar panels and inverters, the output of Pvsyst and PVsol software were similar and did not differ statistically. According to the prepared outputs, in another simulation using the same panel and inverter, the efficiency of the power plant in the east-west delta installation has been entered, and the calculations have been checked. In this case, the installation angle is 25 degrees and simulation algorithms, the Hofmann algorithm for diffuse radiation and the Hey&Davies algorithm were used [29]. The simulation output results show that 7500 panels are needed in this case, and in terms of the required land area, this amount is significantly reduced compared to the previous case and about 9700 square meters are needed. In terms of the performance ratio, there was no significant difference between the delta mode and the southmode, and both simulations were in the same working range. Tables 2 and 3 show the technical specifications of solar panels and inverters used in the simulation. To achieve acceptable results, it has been tried to use the highest quality panel and inverter in this simulation

Table 2. Characteristic of solar panel at STC[b] [36]

Irradiance in W/m^2	200
MPP Voltage in V	40.2
MPP Current in A	2.66
Open Circuit Voltage in V	46
Short-Circuit Current in A	2.8
Fill Factor in %	83.02
Relative Efficiency in %	97.19
Width in mm	1134
Height in mm	2279
Surface in m^2	2.58
Depth in mm	35
Output coefficient in %K	0.036
Maximum System Voltage in V	1500
Incident Angle Modifier (IAM) in %	98

Table 3. characteristics inverter at STC [36]

DC nominal output in kW	50
Max DC Power in kW	66
Nom DC Voltage in V	860
Max Input Voltage in V	1100
Max Input Current in A	90
AC Power Rating in kW	50
Max AC Power in kVA	50
Number of Phases	3
Min Feed in Power in W	250

3. Results & Discussion

The performance ratio is a parameter that can be used to obtain appropriate information about the performance of the solar power plant. Based on the results of the software simulation, the performance ratio in the case of south panels with a fixed base for all months of the year is 0.7 or more, which is considered a suitable ratio (Figure 8).

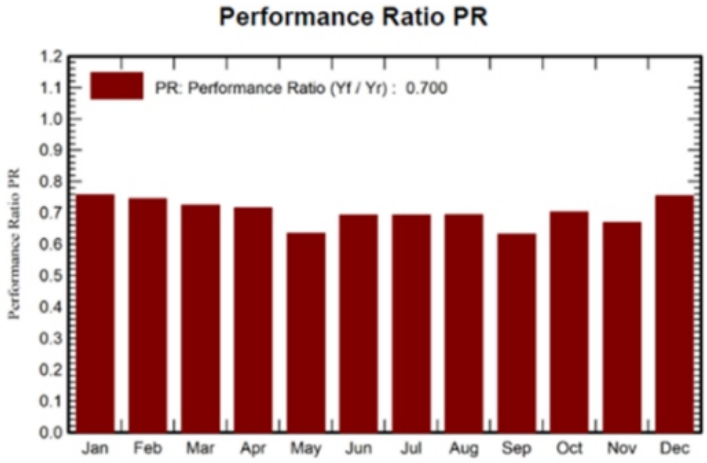

Figure 8. Performance ratio of the installed power plant during the year

For the final monitoring of the process, the simulation performed for the construction of the power plant was evaluated using RETScreen software [32]. Based on the output of the software, the average monthly direct radiation at the installation site is in the range of 120 to 170 kilowatt hours per square meter, which is a suitable value for the start-up and efficiency of the power plant (Figure 9).

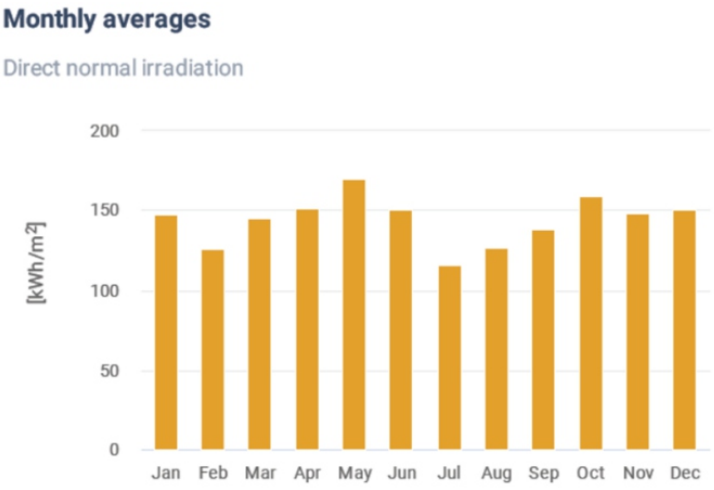

Figure 9. Average direct radiation in the installation position

1259

According to the output and monitoring of the amount of radiation at the site, it was possible to obtain energy from 6:00 AM to 7:00 PM for more than eight months of the radiation year in the installation site, but most of the radiation power in the year is between 8:00 AM and 5:00 PM (Figure 10). Considering that these hours are the peak time for electricity consumption, this is a suitable advantage for the power plant in question. According to the economic estimate made by the software, the investment return time for the installation of this power plant is in the fourth year, and as a result, after four years, the project investor will get a good profit.

In order to obtain the reduction of harmful greenhouse gases, the amount of energy produced by the 4 MW power plant is obtained and compared with the amount of fuel consumed in gas or diesel power plants that produce the same amount of energy a 4 MW. The amount of greenhouse gas produced from the diesel power plant is calculated and expressed as the prevention of greenhouse gas emissions due to the use of the solar power plant. The amount of greenhouse gases removed due to the construction and operation of the mentioned power plant is about 3500 tons (Table 4). Based on the guaranteed purchase price of renewable electricity, the amount of electricity produced by the 4 MW photovoltaic power plant can be calculated by multiplying the amount of electricity produced and the amount of money saved due to the construction and operation of this power plant (Table 4).

The results of the RETScreen environmental simulation have shown that the construction of this solar power plant will lead to a reduction in the production of more than 3500 tons of carbon dioxide. The continuation of the construction of this power plant will have a significant impact on reducing pollution for other industrial estates (Table 4).

Table 4. The amount of carbon dioxide decreased and the income from electricity production

Summary		
	Electriccity export revenue IRR	GHG emission reduction tCO_2
Proposed Case	108,378,851,430	3,499

Average hourly profiles

Direct normal irradiation [Wh/m²]

	Jan	Feb	Mar	Apr	May	Jun	Jul	Aug	Sep	Oct	Nov	Dec
0 - 1												
1 - 2												
2 - 3												
3 - 4												
4 - 5												
5 - 6												
6 - 7			4	69	132	106	46	44	34	31		
7 - 8	69	90	180	266	308	257	150	178	224	279	226	93
8 - 9	390	346	351	398	435	379	256	278	340	449	455	428
9 - 10	512	459	461	504	533	476	341	367	437	550	556	541
10 - 11	590	536	543	573	599	543	410	436	523	626	620	613
11 - 12	626	586	599	607	625	575	451	483	582	670	656	648
12 - 13	636	590	607	604	627	582	469	512	599	663	645	650
13 - 14	612	559	574	581	608	567	466	509	574	610	600	617
14 - 15	559	515	508	523	558	523	428	470	520	540	534	553
15 - 16	477	436	426	428	470	441	347	386	425	439	430	464
16 - 17	280	323	320	319	357	336	248	277	294	253	216	243
17 - 18	3	60	114	157	214	204	127	134	70	18		
18 - 19				4	25	30	14	9				
19 - 20												
20 - 21												
21 - 22												
22 - 23												
23 - 24												
Sum	4753	4499	4688	5034	5491	5020	3751	4082	4623	5129	4938	4850

4. Conclusions

Based on the simulation results, it can be said that it is possible to install this power plant with suitable efficiency and output power of about 3 MW.

Adequate radiation in the study area and relatively low rainfall in this area are the advantages of thedesired location. The absence of local high-speed winds, as well as dust, makes this location a good place to install a power plant Based on the output of the software, installing the panels of this power plant in the form of an eastwest delta will be more cost-effective in terms of finance and also reduce the required surface area compared to the south-facing panel.

The results of the statistical test at the confidence level of 95% between the data output of PVSol and PVSyst software showed that there is no significant difference between the data of the output results, and both software achieved the same answers. The proposal of both soft wares for panel installation was Delta wing panels.

Considering that the purpose of installing and operating this power plant is to use it during peak consumption hours, especially in the hot seasons of the year and the first half of the year, the simulation output shows that the peak efficiency of this power plant is a suitable adaptation. It has peak consumption hours and will eventually help to prevent blackouts in the industrial town. Also, for more than 8 months of the year in this place, it is possible to use this power plant for more than 12 hours, which is also a good advantage for the proposed location. The use of this amount of renewable solar energy in the location of this industrial town will have a significant impact on reducing the amount of pollution. Also, if panels are installed on the roofs of the buildings and sheds in this industrial town, it is possible to obtain the energy needed for current purposes such as lighting, running cooling devices, and security and camera systems. Etc. and this process will also prevent disruptions in the current processes of companies and workshops in the event of a power outage.The most important challenge and limitation in this research have been the justification of the government to establish renewable systems.Considering the climatic conditions of the southern region of Iran, verifying this research and justifying government managers' investments in the renewable energy sector is a difficult task.

Acknowledgements

This research was supported by Hormozgan Regional Electric Company. Authors appreciate colleagues of researh and development as well as energy optimization in building departments who

provided insight and expertise that assisted the research.

Nomenclature

L	Azimuth
δ	height angle
β_N	tilt angle
Ea	extra-terrestrial radiation.
Eext	extra-terrestrial irradiation.
γ_S	Elevation the sun
A_i	anisotropy index
AHP	Analytical Hierarchy Process
IDW	Inverse Distance Weighting
WLC	Weighted Linear Combination
DNI	direct normal irradiance
DEM	Digital elevation Model
STC	Standard Test Conditions
PR	Performance Ratio
GHG	Green House Gas
IRR	Internal Rate Return
MPP	Maximum Power Point
Nom	Nominal
amb	ambient
GCC	Gulf Cooperation Council

References

[1] Zahedi.R, Zahedi.A, Ahmadi.A.(2022), Strategic Study for Renewable Energy Policy, Optimization and Sustainability in Iran, Energy Sustainability, 14(4), 2418-2432, Doi:10.3390/su14042418

[2] Ezzedine. A, Roknabadi.A.R, Mohtashami.G.R. (2021), the Influence of the Geographical Location on the Preventive Replacement of Renewable Energy Devices, Journal of Solar Energy Research, 6(4), 887-897,

[3]Ameze.B.A,Chigozirim.I.J.(2022), Determination of the Optimal Tilt and Azimuth Angle for a Solar Tracking System considering Different Climatic Conditions, Journal of Solar Energy Research, 7(3),1073-1080,

[4] Khazaee.M, Zahedi.R, Faryadras.R, Ahmadi.A .(2022). Assessment of Renewable Energy Production Capacity of Asian Countries: A Review, New Energy Exploitation and Application,1(2),25-41.

[5] Noorollahi.Y, Khatibi.A, Eslami.Sh.(2021). Replacing natural gas with solar and wind energy to

supply the thermal demand of buildings in Iran: A simulation approach, Sustainable Energy Technologies and Assessments, 44, 101047,

[6] Pourarshad.M, Noorollahi.Y, Atabi.Farideh, Panahi.M, (2022). Reducing energy and environmental challenges by modeling clean electricity generation in oil-rich regions. Energy & Environment, https://doi.org/10.1177/0958305X221135056

[7] Lew.G, Sadowska.B, Laskowska.K.C, Zimon.G, Jurkiewicz.M.W,(2021). Influence of Photovoltaic Development on Decarbonization ofPower Generation—Example of Poland.Enerjes,4(22),7819, https://doi.org/10.3390/en14227819

[8] Aksoy.M.H, Calik.M.K.(2022), PERFORMANCE INVESTIGATION OF BIFACIAL PHOTOVOLTAIC PANELS AT DIFFERENT GROUND CONDITIONS, Konya Journal of Engineering Sciences, 10(3),704-718, DOI: 10.36306/konjes.1116729

[9] Narvaez.G, Giraldo.L.F, Bressan.M, Pantoja.A, (2022). The impact of climate change on photovoltaic power potential inSouthwestern Colombia. Heliyon.8,1-8.

[10] Ibrahim.N.A, Alwi.Sh.R.W, Manan.Z.A, Mustsffa.A.A, Kidam.K,(2022). Impact of Extreme Temperature on Solar Power Plant in Malaysia, CHEMICAL ENGINEERING TRANSACTIONS, 94, 343-348,

[11] Al-Baghdadi.M,A.R.S, Ridha.A.A, Al_Khayyat.A.S, (2022). THE EFFECTS OF CLIMATE CHANGE ON PHOTOVOLTAIC SOLAR PRODUCTION IN HOT REGIONS, DIAGOSTYKA.23(3),1-7.

[12] Zahedi.R, Sadeghitabar.E, Ahmadi.A.(2023), Solar energy potential assessment for electricity generation on the south-eastern coast of Iran,future energy, 2(1),15-22,

[13] Rai.A, Shrivastava.A, Jana.K.C, Tripathi.S, Agrawal.A.(2019), Feasibility Analysis of 100 kW Solar Plant for Chandigarh(India), IOP Conf. Series: Materials Science and Engineering 594, doi:10.1088/1757-899X/594/1/012008

[14] Alnaser.N.W, Alnaser.W.E, (2019). The impact of the rise of using solar energy in GCC countries, Renewable Energy and Environmental Sustainability, 4(7),1-11.

[15] Kim.Y, Shin.H.R, Oh.S.H, Yu.K.H,(2022). Analysis on the Economic Feasibility of a Plant Factory Combined with Architectural Technology for Energy Performance Improvement, Agriculture 12,684. https://doi.org/10.3390/agriculture12050684

[16] Talut.M, Bahaj.A.S, James.P,(2022). Solar Power Potential from Industrial Buildings and Impact on Electricity Supply in Bangladesh, Energies, 15, 4037. https://doi.org/10.3390/en15114037 .

[17] Desai.D.D, Raol.J.B, Patal.S,Chauhan.I,(2013), Application of Solar energy for sustainable DairyDevelopment, European Journal of Sustainable Development, 2(4), 131-140.

[18] Behar.O, Pena.R, Kouro.S, Kracht.W,Fuentealba.E, Moran.L, Sbarbaro.D, (2021). The use of solar energy in the copper mining processes: A comprehensive review, Cleaner Engineering and

Technology 4 ,100259.

[19] Farjana.Sh.H, Mahmud.A.A.P, Hida.N,(2020). Solar process heat integration in lead mining process, Case Studies in Thermal Engineering, 22, 100768.

[20] Sánchez-Lozano, J.M., (2014), GIS-based photovoltaic solar farms site selection using ELECTRE-TRI: Evaluating the case for Torre Pacheco, Murcia, Southeast of Spain. Renewable Energy, 66: p. 478-494.

[21] Aydin, N.Y., E. Kentel, and H.S. Duzgun,(2013), GIS-based site selection methodology for hybrid renewable energy systems: A case study from western Turkey , Energy conversion and management, 70: p. 90-106.

[22] Polo, J.,(2015) , Solar resources and power potential mapping in Vietnam using satellite-derived and GIS-based information. Energy conversion and management,. 98: 348-358.

[23] Tercan, E.(2021), A sustainable framework for spatial planning of photovoltaic solar farms using GIS and multi-criteria assessment approach in Central Anatolia, Turkey. Land use policy, 102: p. 105272.

[24] Sun, L.(2021), A GIS-based multi-criteria decision making method for the potential assessment and suitable sites selection of PV and CSP plants. Resources, Conservation and Recycling, 168: p. 105306.

[25] Baghel, N, S. Chander, N.(2022) , Performance comparison of mono and polycrystalline silicon solar photovoltaic modules under tropical wet and dry climatic conditions in east-central India, Clean Energy vol 6, 165–177,

[26] Talut, M. Bahaj ,A, S. James, P. ,(2022), Solar Power Potential from Industrial Buildings and Impact on Electricity Supply in Bangladesh, Energies, 15(11), 4037, 1-17 ,

[27] Taki, M. Najafabadi, M, M.(2019). Technicl and economic evaluation of solar power plant(pothovoltaic) grid-connected(Case stude:1MW power plant in Ahvaz city), Jrenew, 6(1),9-102.

[28] Yosefi, H. Hafefnia, H. Astaraie, F,R.(2016). Feasibility of solar energy to produce electricity in the ocean coasts of southeastern Iran ,The conference on geopolitics, the processing of geopolitical potentials in the development of the southeast coast of the Iran, ((2020),45-59,

[29] George, A,M.(2012). Utility Scale Solar Power Plnts:A GUIDE FOR DEVELPERS AND INVESTORS, International Finance Corporation World Bank Group,(2012),180-185,

[30] Akbari, H. Kavivar, H, R. ,(2018). Optimizing the aspect ratio form and building orientation based on radiation and wind direction (case study: Tabriz, Yazd and Bandar Abbas), Journal of Arid Reions Geographic Studies,9(34), 1-13,

[31] https://globalsolaratlas.info

[32] Komijani, F. Nasolahi, A. Nazari, N. Nahid, Sh. (2014). The Persian Gulf wind analysis using meteorological synoptic stations data, NIVAR,(84-85)38,27-44,

[33] Pron, S. Yavari, Gh. Rezazadeh, M.(2017). Clasification of Hormozgan Province according to liti sky method, Naturl Georaphy,12(46),45-59,

[34] Hofmann. M, Seckmeyer.G.(2017), A New Model for Estimating the Diffuse Fraction ofSolar Irradiance for Photovoltaic System Simulations, Energies 10(2), 248; https://doi.org/10.3390/en10020248

[35]Hofmann. M, Seckmeyer.G.(2017), Influence of Various Irradiance Models and Their Combination on Simulation Results of Photovoltaic Systems, Energies 10(10), 1495;https://doi.org/10.3390/en10101495

[36]https://www.mustsolar.com/category/solarpanel

ISSN. 2476-1234

Numerical Multi-Variable Investigation and Optimization of a High Temperature Hydrogen Production Process Using Solar-Based eliostat Field and Supercritical CO2 Utilization

Hassan Athari, Maghsoud Abdollahi Haghghi *

Department of Mechanical Engineering, Elm-o-Fann University College of Science and Technology, Urmia, Iran

A B S T R A C T

With regard to the sustainability of using carbon dioxide in supercritical processes, this study proposes a novel power/hydrogen cogeneration arrangement consisting of a recompression supercritical carbon dioxide gas turbine cycle and a solid oxide water electrolysis unit in integration with a high-temperature solar-based heliostat field. The steady operation of the system is also guaranteed by means of thermal energy storage tanks. On this path, anumerical multi-variable study and optimization of the entire system are conducted. Hence, four main parameters are viewed to study the sensitivity of the net power output, hydrogen output, energy and exergy efficiencies, and unit cost of products. Hence, a genetic algorithm is applied to investigate the optimum conditions of the entire system considering the maximum energy and exergy efficiencies and the minimum unit cost of products as objective functions. Looking at the results, the sensitivity of the outcomes is further affected by the increase in compressor 1 inlet pressure. Besides, the optimum energy efficiency is 26.81%, optimum exergy efficiency is21.03%, and optimum unit cost of products is 18.79 $/GJ are attainable.

Keywords: *Supercritical CO2 utilization; Solar-based heliostat field; Solid oxide water electrolysis; Multi-variable investigation; Optimization*

1. Introduction

Transitioning from conventional energy conversion routes to updated technologies is absolutely needed to supply the energy demand in different sectors, i.e., urban, industrial, agricultural, etc. [1-3]. Renewable energy-based programs are incredibly increased in recent years; however, further attention is required to identify the most suitable way of energy conversation using renewable energy resources [4,5]. Solar energy is recognized as the zero-emission source of renewable heat-based energy utilized in many projects throughout the world. Different technologies, from low-temperature to high-temperature applications, have been built and evaluated in which high-temperature ones are appropriate for power plants. Solar power tower technology composed of heliostat mirrors and a central receiver is a proper selection for potential cities for power generation and other multigeneration goals [6-9]. To highlight its application, a detailed literature review is represented in the following.

Sezer et al. [10] regarded and studied the advantages of a solar-based heliostat field (SHF) combined with wind turbines for simulation production of heating, cooling, power, and freshwater. They showed an exergy efficiency of 48%. Zoghi et al. [11] evaluated the exergy and costaspects of integrating a SHF,

a biomass gasification subsystem, a gas turbine cycle, low-temperature water electrolysis (LTWE) for hydrogen production, and cooling and heating terminals. So, an exergy efficiency of 43.1% and a total cost rate of products of 7799 $/h were found. Using a SHF, Yuksel et al. [12] investigated a multigeneration process for thesimultaneous production of power, hydrogen, freshwater, cooling, and heating. The proposed system had a higher performance at higher ambient temperatures. Colakoglu and Durmayaz [13] showed the exergy and cost potential of a SHF combined with a gas turbine cycle. The result indicated an exergy efficiency of 34.5% and a levelized cost of products of 0.079 $/kWh. Considering a case study for Qatar, Nedaei et al. [14] proposed a multigeneration process relying on a SHF with net output power and exergy efficiency of 7.4 MW and 38.7%, respectively. Wang et al. [15] showed athermal efficiency between 19.2% and 22% for a SHF integrated with a two-stage recompression gas turbine cycle. In a study by Liang et al. [16], a SHF was used to launch a two-stage recompression supercritical carbon dioxide (S-CO2) gas turbine cycle combined with an organic Rankine cycle (ORC). The most suitable range of net power output was deduced between 2200 kW and 2300 kW. Sachdeva and Singh [17] examined the potential of a combined power plant encompassing a gas turbine cycle, an ORC, and a steam Rankine cycle (STC) in integration with a SHF. This arrangement indicated net power output of 332 kW per unit mass rate of input air of the gas turbine cycle. In a study by Sadeghi et al. [18], the applicability of a SHF combined with a multigeneration system producing power, heating, hydrogen, and oxygen was assessed and investigated. Through the study, they obtained an energy efficiency of 50% and an exergy efficiency of 45%. Keshavarzzadeh et al. [19] designed a SHF combined with a gas turbine cycle for a multigeneration application. They also optimized the operation and found that the optimum unit cost of products was 0.045 $/kWh. Khatoon and Kim [20] utilized supercritical and transcritical Co2-based processes for power generation in combination with a SHF. So, the energy and exergy efficiencies of 42% and 67% were calculated, respectively. Yang et al. [21] used thermal energy storage for a SHF and provided the needed heat for a S-CO2 gas turbine cycle. From their study, energy efficiency was available at 17.1% for winter and 17.8% for summer. Mohammadi et al. [22] considered a combustion chamber and a SHF to launch a recuperative gas turbine cycle. Besides, they stated that fuel consumption and emission decreased considerably.

Green hydrogen production is a valuable method of energy supply for remote areas, which can be considered within multigeneration processes [23-25]. Among available hydrogen production ways, water electrolysis, although an energy-intensive route, has great potential for environmentallyfriendly hydrogen generation [26-30]. A solid oxide electrolyzer cell (SOEC) is a high-temperature waster electrolyzer tool that is suitable for combined processes. Its applicability is reviewed in the following based on some recent studies [31].Mohammadi and Mehrpooya [32] proposed a solarbased process using parabolic dish collectors for hydrogen generation through a SOEC and found that the hydrogen production rate per day and its cost were respectively equal to 41.48 kg/day and 9.1 $/kg. Wang et al. [33] proposed the use of an SOEC in integrating with an engine. The hydrogen production rate was found to be 22.39 kg/h. Hjeij et al. [34] designed a multigeneration process involving hydrogen production. The system also was capable to yield power, heating, ammonia, urea, and natural gas. The hydrogen production rate and total exergy efficiency were obtained to be 0.1 kg/s and 14%, respectively. Xu et al. [35] proposed and optimized a biomass-based steam Rankine cycle combined with a multi-effect desalination and aSOEC. The optimum exergy efficiency and unit cost of products were found to be 17.6% and 26 $/GJ, respectively. Using a SOEC, Alirahmi et al. [36] produced hydrogen via a geothermal-based multigeneration process. They showed that the optimum exergy efficiency was 37.9% and the optimum cost rate of products was 15.1 $/h.

Solar-based arrangements have been reviewed, where there is a gap in introducing high-temperature SOECs in combination with a SHF and S-CO2 gas turbine cycle. On this account, this paper is preparedto design a novel framework for a power andhydrogen cogeneration system using a recompression S-CO2 gas turbine cycle operated by a SHF with thermal energy storage tanks and a SOEC. This study performs a sensitivity study from the thermodynamic and cost standpoints. In addition, a genetic algorithm is used to optimize the proposed process both thermodynamically and

cost standpoints. In addition, a genetic algorithm is used to optimize the proposed process both thermodynamically and economically.

2. Process description

Figure 1 exhibits the schematic of the proposed arrangement in this study. As can be evident, three main parts are there, namely a SHF with storage tanks, a recompression S-CO2 gas turbine cycle, and a SOEC. Since the highest operating temperature of the S-CO2 process is lower than conventional gas turbine cycles, it can be regularly utilized in integration with a SHF. With regard to this ability, it can be represented that such process is proper because the change in the solar status affects the operation of such process less than gas turbine cycles.

First, low-pressure CO2 flows into compressors 1 and 2 at states 1 and 13, respectively. Accordingly, flow 2 passing through the low-temperature recuperator (LTR) is mixed with flow 14 at state 3. So, flow 4 is made and enters the high-temperature recuperator (HTR). Consequently, the pressurized CO2 is further warmed before flowing into the solar unit. Thus, flow 5 goes into storage tank 1 (St.T1),then flow 6 is delivered to the high-pressure turbine (HPT). Subsequently, flow 7 leaves the HPT and is reheated by using storage tank 2 (St.T5). Consequently, the heated CO2 is sent into the lowpressure turbine (LPT). Its output flow at state 9 is the hot flow entering the HTR and LTR. Considering state 18, the heated molten salt (59.5% LiCl / 40.5% KCl) flows into storage tanks at points 19 and 21. Subsequently, these flows are mixed at point 17 and the mixed flow is delivered to the receiver of the SHF. Here, 20% of the power produced by the supercritical process is considered for hydrogen production by the SOEC, and the rest is supplied to the grid.

In the SOEC, water at state 23 is pumped up to state 24, and this flow is delivered to heat exchanger 3 (Hx3). Flow 24 is heated and enters the SOEC after crossing HX3, electrical steam generator (ESG), heat exchanger 2 (HX2), heat exchanger 1 (Hx1), and electrical heater (EH), respectively. Subsequently, flow 29 is mixed with flow 33, and flow 30 is sent into the SOEC. Flow 32 is also sent into heat exchangers 1 and 3 for heat recovery; therefore, the yielded hydrogen is stored at state 35.

3. Materials and Methods

In order to simulate the proposed model, a code has been developed in the engineering equationsolver (EES) software. Afterward, a genetic algorithm has been used to show the optimal operation of the system. EES is a general equationsolving software with the ability to solve thousandsof coupled non-linear algebraic and differential equations numerically. Its other main features include solving

differential and integral equations, do optimization, and provide uncertainty analyses. A major feature of EES is the high accuracy thermodynamic and transport property database that is provided for hundreds of substances in a manner that allows it to be used with the equation solving capability. The input conditions of the simulation are given in Table 1.

Table 1. Input data.

Input parameter	Value
SHF [37]	
DNI, kW/m^2	0.7
Optical efficiency, %	75
Outlet temperature of receiver, ℃	927
Speed of wind, m/s	5
Mirror^' s area, m^2	121
Central receiver area, m^2	60
Emissivity of absorber, (-)	0.88
Number of mirrors, (-)	280
Stefan–Boltzmann constant	5.67×10^{-8}
Recompression S-CO_2 cycle [38]	
Inlet temperature of HPT and LPT, ℃	677
PR of compressor, (-)	2.6
LPT's outlet pressure, bar	76
Isentropic efficiency of turbine, %	90
Isentropic efficiency of compressor, %	88
PPTD of LTR, ℃	5
PPTD of HTR, ℃	10
SOEC [39]	
Operating temperature, ℃	750
Base current density, A/cm^2	1
Outlet pressure, bar	1.15
Area of each cell, m^2	0.324
Pressure loss, %	3
Steam utilization factor, (-)	0.6
Thickness of anode, mm	17.5×10^{-3}
Thickness of cathode, mm	312.5×10^{-3}
Thickness of electrolyte, mm	12.5×10^{-3}
Pre-exponential factor of cathode, A/cm^2	1.344×10^{4}
Pre-exponential factor of anode, A/cm^2	2.051×10^{3}
Activation energy of anode, kJ/mol	120
Activation energy of cathode, kJ/mol	100
Effective diffusion coefficient at anode, m^2/s	2×10^{-5}
Effective diffusion coefficient at cathode, m^2/s	5.11×10^{-5}
Effectiveness of heat exchangers	0.97
Pump isentropic efficiency, %	80

Furthermore, some base assumptions are regarded as follows [37-39]:

The temperature and pressure of the reference state are T0 = 25 oC and P0 = 1 bar.

The operation of the system is at steady-state.

The pressure drop of the piping network and heat exchangers is zero.

The kinetic and potential forms of energy and exergy are zero.

Turbine, pumps, and compressors are adiabatically modelled with a specific isentropic efficiency.

The operating temperature of the SOEC fixed.

3.1. Thermodynamic analysis

For each component, the mass balance equation and the first law of thermodynamics (energy balance) are mathematically given as [46]:

$$\dot{Q} - \dot{W} = \sum \dot{m}_{out} h_{out} - \sum \dot{m}_{in} h_{in} \qquad (1)$$

$$\sum \dot{m}_{out} = \sum \dot{m}_{in} \qquad (2)$$

where $\dot{m}$ denotes the mass flow rate, h denotes the

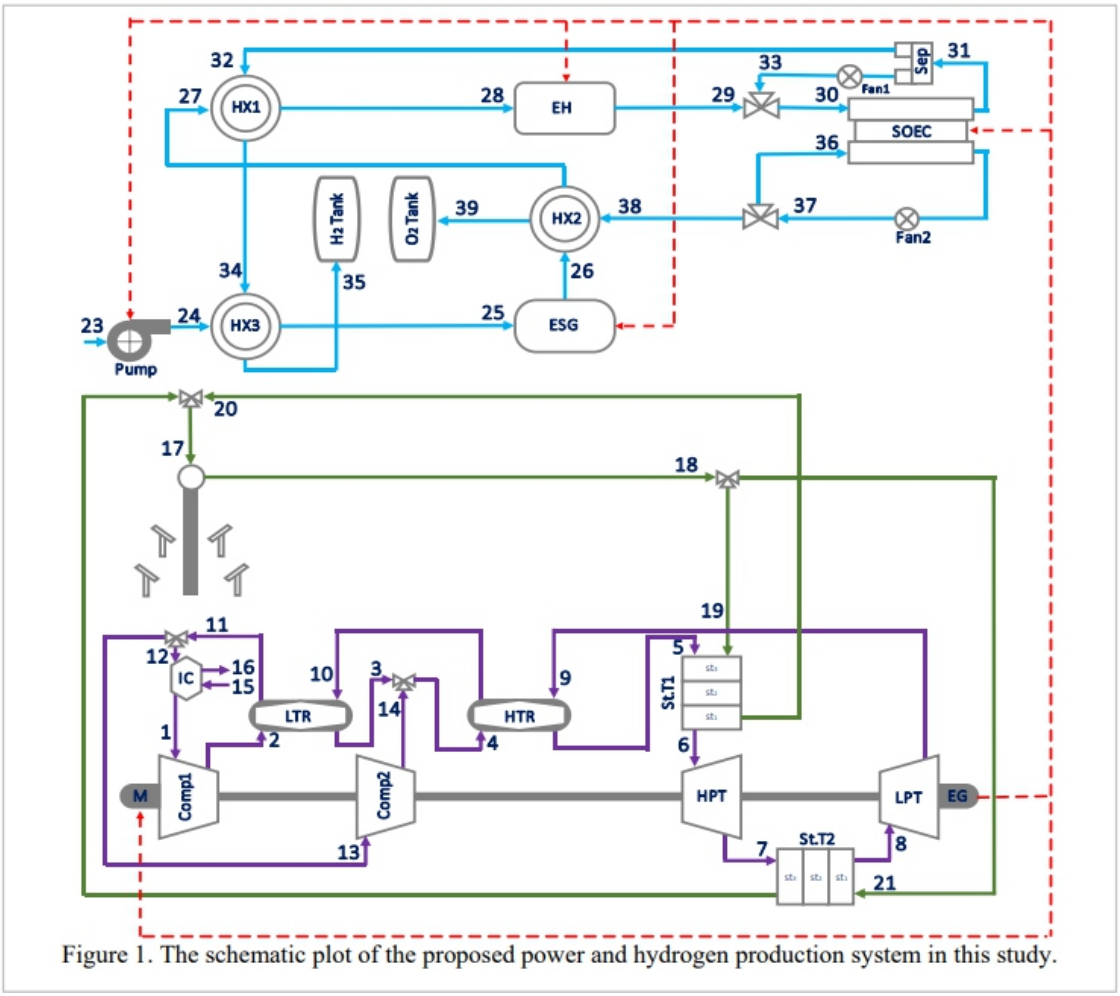

Figure 1. The schematic plot of the proposed power and hydrogen production system in this study.

specific enthalpy, $\dot{W}$ denotes the work, and $\dot{Q}$ denotes the heat transfer rate.

In addition, the second law of thermodynamics (exergy account) is formulated as [46]:

$$\dot{E}_d = \sum\left(1-\frac{T_0}{T_j}\right)\dot{Q}_j - \dot{W}_{cv} + \sum\dot{E}_{in} - \sum\dot{E}_{out} \quad (3)$$

where $\dot{E}_d$ denotes the exergy destruction rate.

Here, the exergy rate of each flow is calculable based on the physical ($\dot{E}_{ph}$) and chemical ($\dot{E}_{ch}$) exergy rates [46].

$$\dot{E} = \dot{E}_{ph} + \dot{E}_{ch} \quad (4)$$

$$\dot{E}_{ph} = \sum\dot{m}_i \times\left[\left(h_i - h_0\right) - T_0\left(s_i - s_0\right)\right] \quad (5)$$

$$\dot{E}_{ch} = \dot{n}\left[\sum y_m \bar{e}_m^{ch,0} + \bar{R}T_0\sum y_m \ln\left(y_m\right)\right] \quad (6)$$

Here, $\bar{R}$ denotes the universal gas constant, s denotes the specific entropy, y_m denotes the molar fraction of species m, and $\bar{e}_m^{ch,0}$ denotes its standard molar chemical exergy.

3.2. Solar-based heliostat field

The process of the SHF is definable via determining the solar input energy ($\dot{Q}_{SHF,in}$), gained useful energy ($\dot{Q}_{SHF,u}$), and energy loss ($\dot{Q}_{SHF,L}$). The rate of gained useful energy equals the difference between solar input energy and energy loss as follows [12,14,37]:

$$\dot{Q}_{SHF,u} = \dot{Q}_{SHF,in} - \dot{Q}_{SHF,L} \quad (7)$$

Here, the solar input energy is attainable by:

$$\dot{Q}_{SHF,in} = \eta_F DNI A_{mi} N_{mi} \quad (8)$$

where A_{mi} denotes the area of each mirror, N_{mi} denotes the number of mirrors, η_F denotes the optical efficiency, and DNI denotes the direct normal irradiation.

Here, energy loss depends on the radiation thermal loss ($\dot{Q}_{RAD}$), convection thermal loss ($\dot{Q}_{CONV}$), and reflection thermal loss ($\dot{Q}_{REF}$) [12,14,37].

$$\dot{Q}_{SHF,L} = \dot{Q}_{RAD} + \dot{Q}_{CONV} + \dot{Q}_{REF} \quad (9)$$

The radiation thermal loss is functioned as [12,14,37]:

$$\dot{Q}_{RAD} = \varepsilon\sigma A_{rec} F_r\left(T_{rec}^4 - T_a^4\right) \quad (10)$$

$$F_r = \frac{A_{ape}}{A_{rec}} \quad (11)$$

where σ denotes the Stefane-Boltzmann constant, $\boldsymbol{\varepsilon}$ denotes the emissivity coefficient, F_r denotes the view factor, T is the temperature, and A is the area. Here, subscript a, rec, and ape respectively denote ambient, receiver, and aperture.

Moreover, the convection thermal loss is defined as [12,14,37]:

$$\dot{Q}_{CONV} = h_{air,for,insi} A_{ape}\left(T_{rec} - T_a\right) \quad (12)$$

$$h_{air,for,insi} = 10.45 - V_{wind} + 10\sqrt{V_{wind}} \quad (13)$$

where $h_{air,for,insi}$ denotes the forced heat transfer coefficient and V_{wind} denotes the wind velocity.

Finally, reflection thermal loss equals:

$$\dot{Q}_{REF} = \dot{Q}_{SHF,in} F_r \rho_{rec} \quad (14)$$

where ρ_{rec} denotes the reflectivity coefficient of the receiver.

Referring to Ref. [40], storage tanks can be modelled in three different parts. Therefore, the following relations are utilized [40].

$$\frac{\rho V_{st}}{3} C_P \frac{dT_{st,1}}{dt} = \dot{m}_{MS} C_{P,MS}\left(T_{MS,in} - T_{st,1}\right) + \dot{m}_{CO_2} C_{P,CO_2}\left(T_{st,2} - T_{st,1}\right) - U_{st} A_{st,1}\left(T_{st,1} - T_a\right) \quad (15)$$

$$\frac{\rho V_{st}}{3} C_P \frac{dT_{st,2}}{dt} = \dot{m}_{MS} C_{P,MS}\left(T_{st,1} - T_{st,2}\right) + \dot{m}_{CO_2} C_{P,CO_2}\left(T_{st,3} - T_{st,2}\right) - U_{st} A_{st,2}\left(T_{st,2} - T_a\right) \quad (16)$$

$$\frac{\rho V_{st}}{3} C_P \frac{dT_{st,2}}{dt} = \dot{m}_{MS} C_{P,MS}\left(T_{st,2} - T_{st,3}\right) + \dot{m}_{CO_2} C_{P,CO_2}\left(T_{VG2,out} - T_{st,3}\right) - U_{st} A_{st,2}\left(T_{st,3} - T_a\right) \quad (17)$$

Based on Ref. [40], the unsteady terms in above-mentioned equations are neglectable.

Also [40],

$$T_{st,3} = T_{MS,out} \quad (18)$$

$$T_{st,1} = T_{CO_2,out} \quad (19)$$

In addition, the introduced areas are computed as [40]:

$$A_{st,1} = \frac{\pi D_{st}^2}{4} + \frac{\pi D_{st} L_{st}}{3} \quad (20)$$

$$A_{st,2} = \frac{\pi D_{st} L_{st}}{3} \quad (21)$$

$$A_{st,3} = \frac{\pi D_{st}^2}{4} + \frac{\pi D_{st} L_{st}}{3} \quad (22)$$

where [40]

Here, $\Delta\bar{g}^{\circ}$ denotes the Gibbs free energy difference of the reaction and T_{SOEC} denotes the SOEC's operating temperature.

$$L_{st} = \frac{D_{st}}{2} \quad (23)$$

$$V_{st} = \frac{A_{mi} N_{mi}}{30} \quad (24)$$

3.3. Solid oxide electrolyzer cell

The hydrogen production reaction of the SOEC is written as [39]:

$$H_2O \rightarrow 2H^+ + \frac{1}{2}O_2 + 2e^- \quad (25)$$

Hence, the molar rate of the hydrogen, water, and oxygen at the outlet state of the SOEC are formulated as [39]:

$$\dot{n}_{H_2,out} = \frac{J_{SOEC} N_{SOEC} A_{SOEC}}{2F} \quad (26)$$

$$\dot{n}_{O_2,out} = 0.5 \times \frac{J_{SOEC} N_{SOEC} A_{SOEC}}{2F} \quad (27)$$

$$\dot{n}_{H_2O.out} = \dot{n}_{H_2O.in} - \dot{n}_{H_2O.utilized} \quad (28)$$

$$\dot{n}_{H_2O,utilized} = \frac{J_{SOEC} N_{SOEC} A_{SOEC}}{2F} \quad (29)$$

where J_{SOEC} denotes the current density, A_{SOEC} denotes the cell area, N_{SOEC} denotes the number of cells, and F denotes the Faraday constant.

Additionally, the factor of steam utilization (U_{steam}) is crucial to perform the SOEC's molar balance. So, U_{steam} can be formulated as [39]:

$$U_{steam} = \frac{\dot{n}_{H_2O,utilized}}{\dot{n}_{H_2O,in}} \quad (30)$$

Afterward, cell voltage of the SOEC is fundable by the sum of the Nernest voltage (V_N) and voltage loss (V_L) [39]:

$$V_{SOEC} = V_N - V_L \quad (31)$$

where [39]

$$V_N = -\frac{\Delta \bar{g}^\circ}{2F} + \frac{\bar{R} T_{SOEC}}{2F} \ln\left(\frac{P_{O_2,an}^{0.5} P_{H_2,ca}}{P_{H_2O,ca}}\right) \quad (32)$$

$$\Delta \bar{g}^\circ = \bar{g}^\circ_{H_2O} - \bar{g}^\circ_{H_2} - 0.5\bar{g}^\circ_{O_2} \quad (33)$$

$$\bar{g}^\circ = \bar{h} - T_{SOEC}\bar{s}^\circ$$

Thermoeconomics is a cost-based evaluation method suitable for energy systems based on the exergy, total investment cost ($\dot{Z}_{tot}$), and cost of input fuel ($\dot{C}_{fuel}$).

Also, the voltage loss equals [39]:

$$V_L = V_{ohm} + V_{act} + V_{conc} \quad (35)$$

Ohmic voltage (V_{ohm}) depends on the component i's thickness (δ_i), and constant variables A and B [39].

$$V_{ohm} = J_{SOEC} \cdot \left[A_i \delta_i \times exp\left(\frac{B_i}{T_{SOEC}}\right)\right] \quad (36)$$

The activation voltage loss (V_{act}) is available by [39]:

$$V_{act} = V_{act,a} + V_{act,c} \quad (37)$$

$$V_{act,a} = \frac{\bar{R} T_{SOEC}}{2F} \sinh^{-1}\left(\frac{J_{SOEC}}{2J_{o,a}}\right) \quad (38)$$

$$V_{act,c} = \frac{\bar{R} T_{SOEC}}{2F} \sinh^{-1}\left(\frac{J_{SOEC}}{2J_{o,c}}\right) \quad (39)$$

$$J_o = \gamma_i \exp\left(-\frac{E_{act}}{\bar{R} T_{SOEC}}\right) \quad (40)$$

where γ denotes the pre-exponential factor and J_o denotes the exchange current density.

Moreover, the concentration voltage loss (V_{conc}) is formulated as [39]:

$$V_{conc} = V_{conc,a} + V_{conc,c} \quad (41)$$

$$V_{conc,a} = \frac{\bar{R} T_{SOEC}}{2F} \ln\left[\left(1 + \frac{J_{SOEC} \bar{R} T_{SOEC} \delta_a}{2F D_a^{eff} P_{O_2,a}}\right)^{0.5}\right] \quad (42)$$

$$V_{conc,c} = \frac{\bar{R} T_{SOEC}}{2F} \ln\left(\frac{1 + \frac{J_{SOEC} \bar{R} T_{SOEC} \delta_c}{2F D_c^{eff} P_{H_2,c}}}{1 - \frac{J_{SOEC} \bar{R} T_{SOEC} \delta_c}{2F D_c^{eff} P_{H_2O,c}}}\right) \quad (43)$$

where D^{eff} denotes the effective diffusion coefficient.

Consequently, the required power by the SOEC is obtained as [39]:

$$\dot{W}_{SOEC} = N_{SOEC} J_{SOEC} A_{SOEC} V_{SOEC} \quad (44)$$

Its input power is provided from the recompression S-CO_2 gas turbine cycle and equals 20% of its net power output.

3.4. Thermoeconomic analysis

Pump

$$Z_{pump} = 1266\left(\frac{\dot{W}_{pump}}{1000}\right)^{0.71}\left(1 + \frac{0.2}{1 - \eta_{pump}}\right)$$

Subsequently, the investment cost should be updated using the chemical index of the present year (CI_{PY}) and reference year (CI_{RY}) as below [47]:

The total investment cost is definable as the sum of the investment cost of all components.

For a known component, the investment cost is equal to [47]:

$$\dot{Z} = Z\frac{CRF}{N}\varphi \tag{45}$$

Here, Z denotes the purchase cost (see Table 2), CRF denotes the capital recovery factor, φ denotes the maintenance factor, and N denotes time of operation during the year.

CRF depends on the lifetime (n) and interest rate (i_r) of the system as follows [47]:

$$CRF = \frac{i_r\,(1+i_r)^n}{(1+i_r)^n\text{-}1} \tag{46}$$

Table 2. Investment cost function of devises [41-43].

Device	Relevant equation
SHF	$Z_{SHF} = Z_{rec} + Z_{Hel}$
	$Z_{rec} = A_{rec}\left(79\times T_{rec} - 42000\right)$
	$Z_{Hel} = 150\times N_{mi}A_{mi}$
St.T	$Z_{St.T} = 494.09 + 808\times V_{st.T}$
Tur	$Z_{tur} = \frac{479.34\times \dot{m}_{in}}{0.92-\eta_{GT}}\ln\left(\frac{P_{out}}{P_{in}}\right)\times\left[1+\exp\left(0.036\times T_{GT}-54.4\right)\right]$
EG	$Z_{EG} = 26.18\left(\dot{W}_{EG}\right)^{0.95}$
Comp	$Z_{comp} = \frac{71.1\times \dot{m}_{in}PR_{comp}}{0.9-\eta_{AC_1}}\ln\left(PR_{comp}\right)$
Motor	$Z_M = 26.18\left(\dot{W}_M\right)^{0.95}$
Recu	$Z_R = 12000\left(\frac{A_R}{100}\right)^{0.6}$
SOEC	$Z_{SOEC} = A_{SOEC}N_{SOEC}\left(2.96\times T_{SOEC}-1907\right)$
HX	$Z_{HX} = 130\left(\frac{A_{HX}}{0.093}\right)^{0.78}$
IC	$Z_{IC} = 12000\left(\frac{A_{IC}}{100}\right)^{0.6}$

biological evolution. This algorithm alters the population of individual solutions iteratively. The genetic algorithm picks individuals at random from the existing population at each stage and employs them as parents to create offspring for the following generation [45]. The population "evolves" toward the best option over the course of subsequent generations. The algorithm is available for optimization via the EES software. The objective functions put forwards herein include overall energy efficiency (η_{en}), overall exergy efficiency (η_{ex}), unit cost of products and ($c_{product}$) of the system.

$$\dot{Z}_{updated} = \dot{Z}\frac{CI_{PY}}{CI_{RY}} \tag{47}$$

3.5. Performance variables

The current study investigates five main performance variables formulated in the following.

First, the net power output equals [46]:

$$NPO = \dot{W}_{EG} - \dot{W}_M - \dot{W}_{SOEC} - \dot{W}_{ESG} - \dot{W}_{EH} - \dot{W}_{pump} \tag{48}$$

Also, the hydrogen output is found as [46]:

$$HO = 24\times 3600\times\frac{\dot{m}_{35}}{\rho_{H_2}} \tag{49}$$

Consequently, the energy and exergy efficiencies are obtainable as [46]:

$$\eta_{en} = \frac{NPO + \dot{m}_{35}LHV_{H_2}}{\eta_F DNIA_{mi}N_{mi}} \tag{50}$$

$$\eta_{ex} = \frac{NPO + \dot{m}_{35}e^{ch,0}_{H_2}}{DNIA_{mi}N_{mi}\left[1+\left(\frac{1}{3}\right)\left(\frac{T_0}{T_s}\right)^4-\left(\frac{4}{3}\right)\left(\frac{T_0}{T_s}\right)\right]} \tag{51}$$

Finally, products' unit cost of the system is equal to [47]:

$$c_{product} = \frac{\dot{Z}_{tot}}{NPO + \dot{E}_{35}} \tag{52}$$

3.6. Optimization

Optimizing the performance of energy systems to find an optimal balance between thermodynamic efficiency and costs can elicit cost reduction in addition to lasting stability. Accordingly, this part aims to present an optimization model to determine the optimal functioning of the system. Among different methods, herein the genetic algorithm structure as an evolutionary method is employed for optimizing the system [44]. Figure 2 shows the relevant flowchart. The genetic algorithm uses the natural selection process to solve constrained and unconstrained optimization problems, simulating

We considered a comprehensive parametric study and concluded that decision variables selected in equations 53-56 have the highest impact on the main objectives. So, these variables have been chosen for optimization. Also, we considered these parameters and their limitation range according to two main points. At first, we regarded similar studies; second to that, we considered the limitations of the simulation governing our new proposed system.

The optimization function is shown as follows if the objective function is decided to be the overall

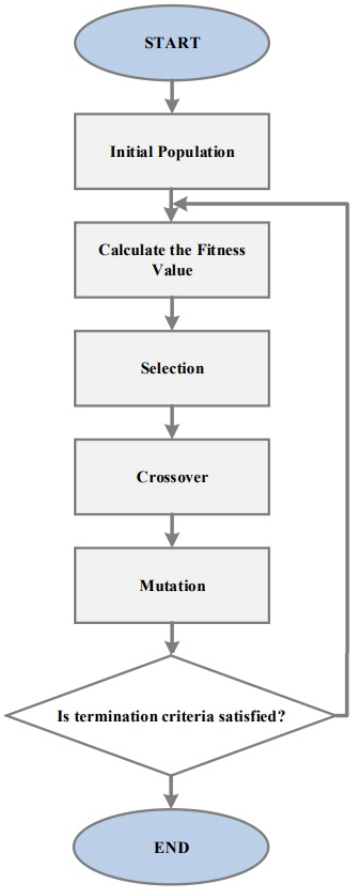

Figure 2. The flowchart of the genetic algorithm.

In this regard, the decision variables and their range of change are introduced below:

$$2.4 \le PR_{copm} \le 4 \ (-) \quad (53)$$

$$665 \le T_{in,tur} \le 710 \ (^{\circ}C) \quad (54)$$

$$75 \le P_1 \le 90 \ (\text{bar}) \quad (55)$$

$$0.4 \le J_{SOEC} \le 1.3 \ (A/cm^2) \quad (56)$$

20.78 to 21.37 $/GJ. This trend is a consequence of decreased exergy level of products.

In addition, according to Table 4, the accurate simulation of the SOEC is visible. Here, the data obtained by AlZahrani and Dincer [39] are considered for validation. So, the model is verified by a total error below 1%.

Table 4. Model validation of the SOEC with Ref. [39].

J_{SOEC} (A/cm^2)	This study	Ref. [39]
	Power density (A/m^2)	
0.3	3.26	3.2
0.4	4.43	4.2

energy efficiency:

Maximize (EnOM): EnOM = η_{en} {Based on decision variables} (57)

If overall exergy efficiency is determined as the objective function, the optimization function is presented as:

Maximize (ExOM): ExOM = η_{ex} {Based on decision variables} (58)

If the $c_{product}$ is set as the objective function, then:

Minimize (COM): COM = $c_{product}$ {Based on decision variables} (59)

To do this, number of generations, number of individuals, mutation rate, and crossover are respectively set as 64, 32, 0.2, and 0.8, respectively.

4. Results and discussion

This section is provided in three parts, validation, sensitivity study, and optimization results.

4.1. Validation

Tables 3 and 4 respectively show the validity of the model of the SHF and SOEC in this study. As Table 3 depicts, the efficiency of the receiver is evaluated based on different solar irradiations and is compared with those reported by Xu et al. [37]. Here, the selected rang for the *DNI* is between 0.2 kW/m^2 and 1.0 kW/m^2, and the obtained total error is below 1%.

Table 3. Model validation of the SHF with Ref. [37].

DNI (kW/m^2)	This study	Ref. [37]
	η_{rec} (%)	
0.2	43.0	45.0
0.4	49.5	50.0
0.6	53.0	54.0
0.8	55.0	56.0
1.0	57.0	58.0

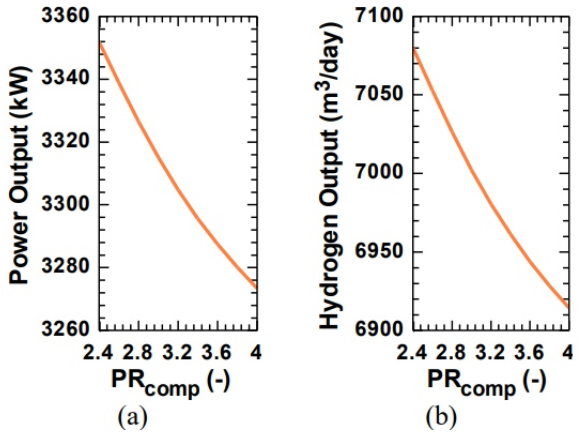

0.5	5.62	5.5
0.6	6.85	6.9
0.7	8.10	8.15
0.8	9.38	9.6
0.9	10.69	10.5
1.0	12.02	11.9

4.2. Parametric study

In the present work, the parametric study is performed with respect to the variation in important thermodynamic and thermoeconomic variables, including *NPO, HO,* η_{en}, η_{ex}, and $c_{product.}$ In addition, the studied parameters are given in equations 53-56. Plots 3-6 exhibit the pertinent results.

In Figure 3, the evaluated variables are measured against PR_{comp} ranging from 2.4 to 4. From Figures 3a and 3b, *NPO* increases and *HO* decreases. The increase in the PR_{comp} diminishes the CO_2 mass flow rate, so the power produced by the HPT goes up while LPT's capacity goes down. Due to the higher impact of the LPT's capacity on the *NPO*, this variable decreases from 3352 to 3273 kW. As previously pointed out, the SOEC subsystem receives its input power from the recompression S-CO_2 gas turbine cycle. Owing to the reduction in its power output, the rate of electrochemical reaction reduces; as a result, *HO* declines from 7080 to 9614 m^3/day. According to Figures 3b and 3c, both thermodynamic efficiencies, i.e., η_{en} and η_{ex}, face a drop. This trend strongly depends on the reduction in the level of products with PR_{comp}. Hence, η_{en} reduces from 23.89% to 23.33% and η_{ex} from 19.09% to 18.65%. From the economic perspective, as Figure 3d shows, higher evaluated pressure ratios are inappropriate by which the $c_{product}$ escalates from

However, the difference between the produced power and consumed power increases, so *NPO* experiences an increase from 3303 to 3429 kW. Consequently, the *HO* also enhances from 6977 to 7943 m^3/day (see Figure 4b). Higher productivity of products leads to proper thermodynamic performance at higher temperatures. As Figures 4c and 4d depict, η_{en} and η_{ex} increase from 23.45% and 18.81% to 24.44% and 19.53%, respectively. This means that the irreversibility of the system reduces with $T_{in,tur}$, so $c_{product}$ experiences a reduction from 21.10 to 20.12 $/GJ.

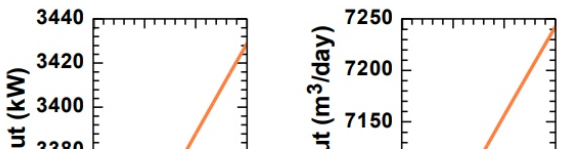

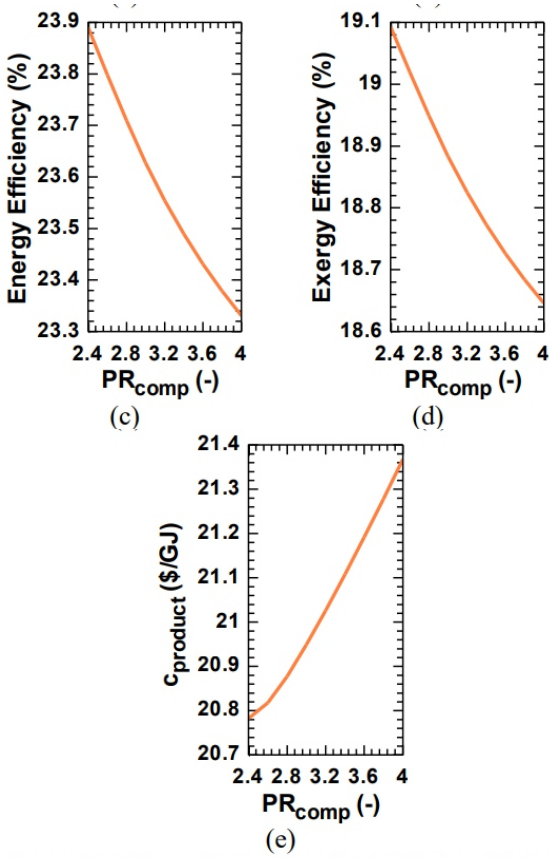

Figure 3. Effect of PR_{comp} on the studied variables.

The behaviour of the studied performance variables based on $T_{in,tur}$ (from 665 to 710 °C) is investigated in Figure 4. As can be seen, enhancing this variable positively affects the productivity and cost measures of performance. According to Figure 4a, although the enthalpy difference of both turbines increases affected by this change, the CO_2 mass flow rate drops. Therefore, the power yielded by turbines and power supplied to compressors decline.

The influence of increasing P_1 from 75 to 90 bar on the investigated performance variables is visible in Figure 5.

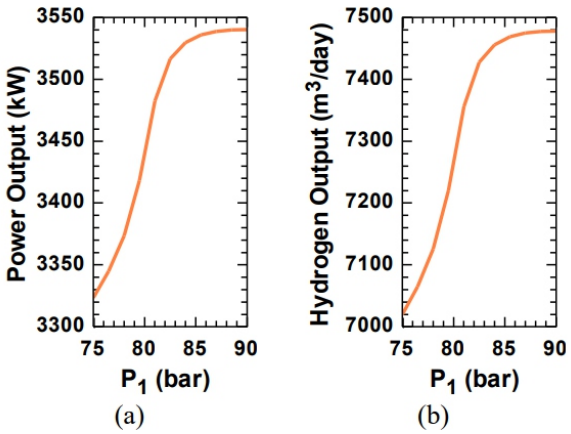

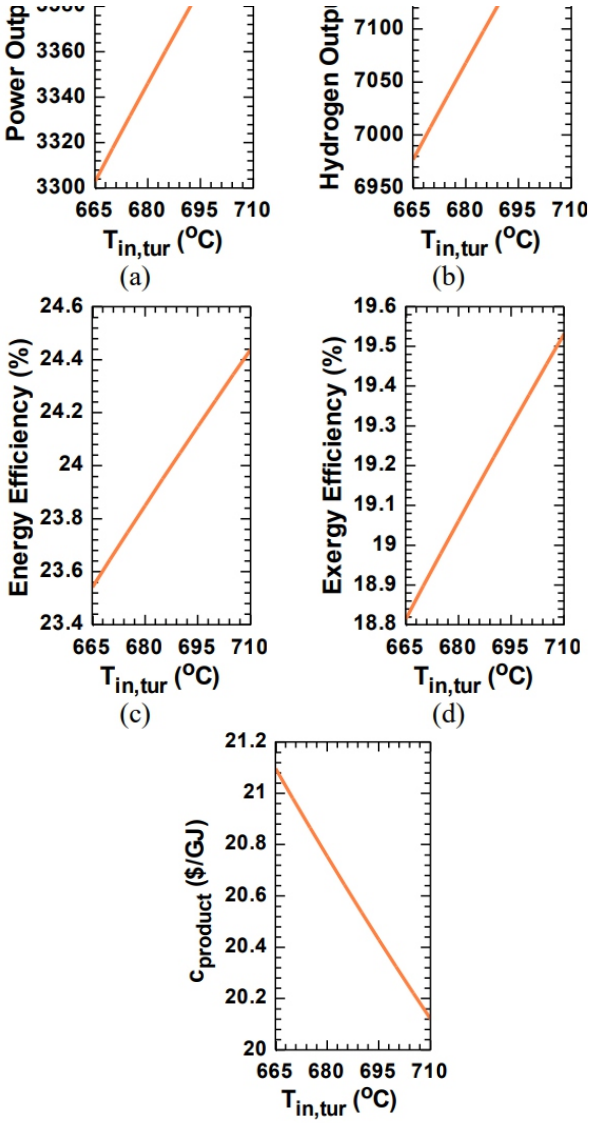

Figure 4. Effect of $T_{in,tur}$ on the studied variables.

further power with increasing P_1. Consequently, *NPO* rises from 3323 to 3540 kW, and *HO* from 7020 to 7478 m^3/day. Referring to Figures 5c and 5d, η_{en} and η_{ex} upsurge from 23.69% and 18.93% to 25.23% and 20.17%, correspondingly. From Figure 5e, it is deduced that higher pressures at state 1 cause lower $c_{product}$ because the exergy ability of the system enhances. So, $c_{product}$ declines from 20.92 to 19.61 $/GJ.

Figure 6 indicates the effect of the last studied parameter, i.e., J_{SOEC} (from 0.4 to 1.3 A/cm^2), on the performance variables. This variation affects *HO* at first owing to the variation in N_{SOEC} and V_L. Indeed, V_L enhances with growing the J_{SOEC}; however, because of the constant SOEC's power input, N_{SOEC} and the mass flow rate of the water input diminish, as well. Therefore, *HO* reduces from 7653 to 6818 m^3/day. Also, the power supplied to the ESG and EH witnesses a decrement, resulting an increment in the *NPO* from 3329 to 3340 kW. The reduced *HO* not only causes a reduction in energy and exergy levels

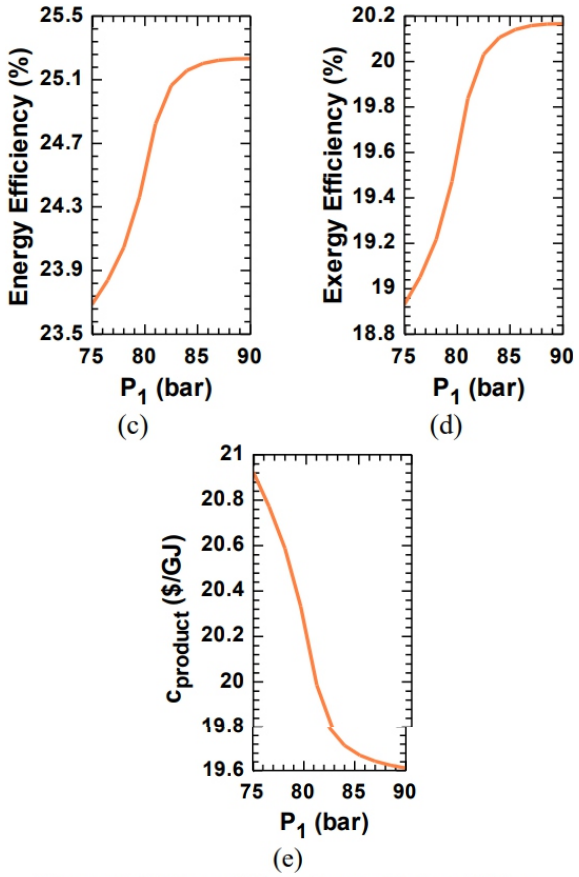

Figure 5. Effect of P_1 on the studied variables.

With this increase, the CO_2 mass flow rate at the outlet of the LPT upsurges. Also, the inlet mass flow rate of Comp1 decreases and of Comp2 increases, so their consumed power decreases and increases, respectively. Hence, the total power consumption capacity of the recompression S-CO_2 gas turbine cycle reduces. Furthermore, HPT is able to produce

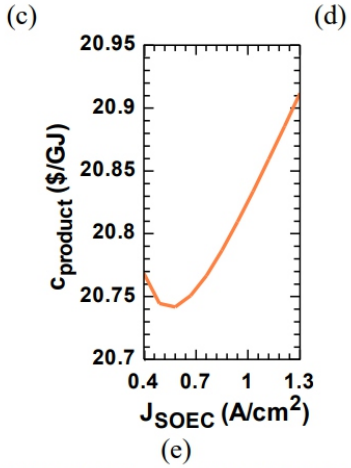

Figure 6. Effect of J_{SOEC} on the studied variables.

4.3. Optimization results

This study utilized a genetic algorithm to optimize the operation of the system in three

of products, but also increases the irreversibility of the processes, so both efficiencies decline. Here, η_{en} and η_{ex} descend from 24.17% and 19.31% to 23.64% and 18.89%, correspondingly. Looking at Figure 5e, $c_{product}$ faces a slight reduction at first, then rises up to 20.91 \$/GJ at 1.3 A/cm^2.

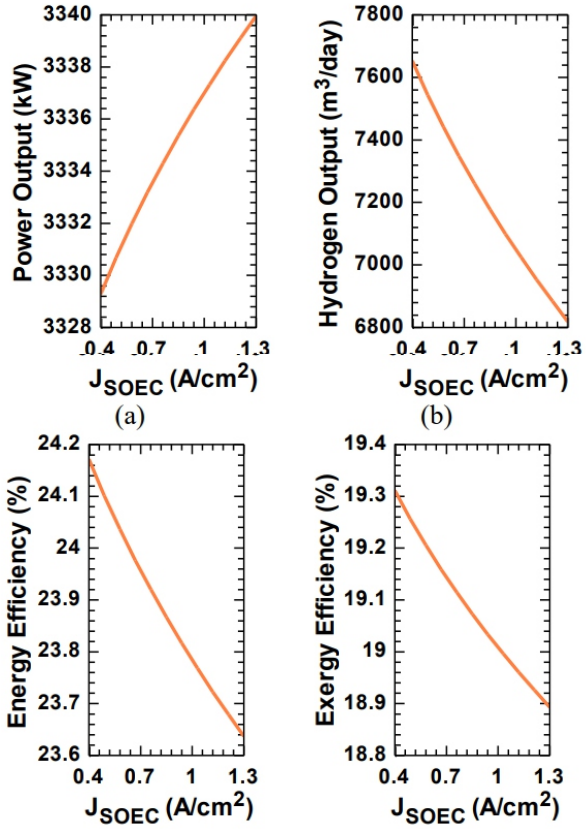

proposed system at the optimum state based on exergy efficiency (ExOM). As can be seen, the highest exergy destruction rate belongs to the HSF, where the total exergy destruction rate of this component is computed to be 20667 kW. After that, HTR and storage tank 1 have the second- and third-highest exergy destruction rates of 595.5 kW and 245.7 kW, respectively.

different scenarios, namely EnOM, ExOM, and COM. The selected decision parameters are completely discussed in equations 53-56. Hence, Table 5 indicates the relevant outcomes. Based on this table, the η_{en} of the EnOM equals 26.81%; this variable is 3.03 percent-point higher than base case. Referring to the second case (ExOM), η_{ex} is obtained to be 21.03; 2.02 percent-point higher than base case. In the last case (COM), $c_{product}$ is found to be 18.79 \$/GJ which is 9.8% better than the base case. The highest *NPO* is attained to be 3610 kW correspondent to the first optimum case. In addition, the highest *HO* is equal to 8266 m^3/day visible in the second optimization case (ExOM).

Table 5. Optimization results of decision parameters and performance variables.

Parameter	Base	EnOM	ExOM	COM
PR_{comp} (-)	2.63	3.21	3.32	3.43
$T_{in,tur}$ (°C)	676.9	708.9	709.9	709.9
P_1 (bar)	76.0	85.2	86.1	87.1
J_{SOEC} (A/cm^2)	1.00	0.41	0.40	0.53
NPO (kW)	3337	3610	3583	3410
HO (m^3/day)	7049	8221	8266	8079
η_{en} (%)	23.78	26.81	26.01	25.05
η_{ex} (%)	19.01	20.76	21.03	20.89
$\dot{Z}_{tot}$ (\$/h)	315.6	319.1	317.2	313.5
$c_{product}$ (\$/GJ)	20.83	19.28	18.99	18.79

Figure 7 indicates the results of the exergy destruction rate for established components of the thermodynamic and thermoeconomic points of view and optimized using a genetic algorithm. Three different optimization cases (EnOM, ExOM, and COM) are considered and evaluated. The main findings of the study are as follows:

- Referring to the parametric study, the sensitivity of the studied performance variables was more changed with increasing P_1.

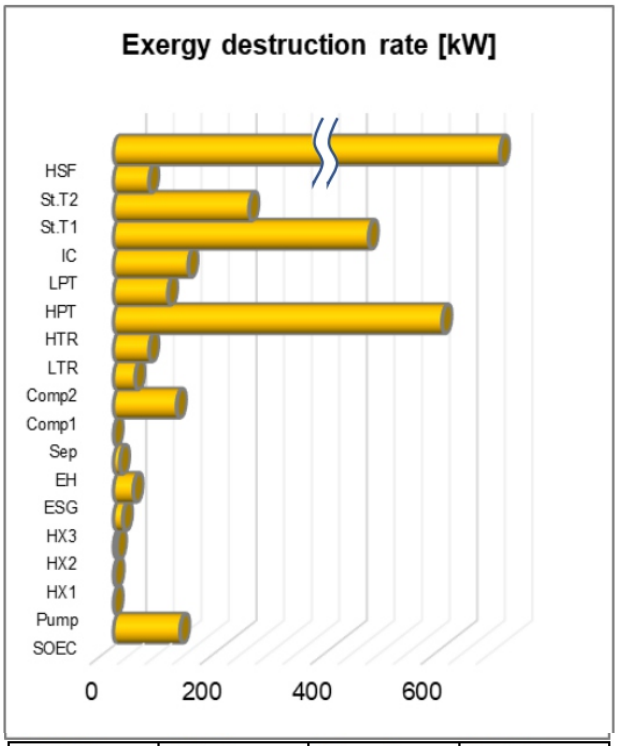

SOEC	120.5	Comp2	39.16
Pump	3.09E-05	LTR	64.51
HX1	1.584	HTR	595.5
HX2	5.806	HPT	98.54
HX3	16.79	LPT	135.4
ESG	35.83	IC	462.3
EH	11.52	St.T1	245.7
Sep	0	St.T2	64.43
Comp1	114.3	SHF	20667

Figure 7. Exergy destruction rate of components at ExOM mode.

5. Conclusions

This study presented an innovative high-temperature cogeneration system producing power and hydrogen using solar energy. The system comprised a solar-based heliostat field (SHF), a recompression supercritical carbon dioxide (S-CO_2) gas turbine cycle, and a solid oxide electrolyzer cell (SOEC). The proposed system was examined from

- The increase in the PR_{comp} led to a decline in the production capacity of products and η_{en} and η_{ex}. Also, $c_{product}$ increased continuously.
- Higher $T_{in,tur}$ and P_1 were thermodynamically and economically useful. They increased the productivity, both efficiencies, and decreased the $c_{product}$.
- With increasing the J_{SOEC}, HO, η_{en}, and η_{ex} reduced, whereas NPO faces an increment. The $c_{product}$ declined at first, then increased.
- The optimum η_{en} was equals 26.81%; 3.03 percent-point higher than base case. Also, the optimum η_{ex} was 21.03; 2.02 percent-point higher than base case. Moreover, the optimum $c_{product}$ was calculated at 18.79 \$/GJ which is 9.8% better than the base case.

The most crucial limitations of the proposed design depend on the establishment and use of equipment and control of thermodynamic conditions. In detail, limited access to solar energy and unstable radiations can create problems for sustainable operation. On the other hand, reserved devices should be available to increase the life of the system and respond to specific conditions. Due to the structure of the system, expert supervisory workforces are also required permanently. In addition, from the thermodynamic operating conditions, controlling the solar status through storage tanks is critical for the stability of the proposed process.

For further studies, since the proposed process for the HSF subsystem has a high thermal-environmental potential compared to similar studies in the literature, it is suggested to investigate the use of available solar energy in each climatic with a case study approach. In addition, a life cycle assessment can be useful to show the performance of the proposed system completely.

Nomenclator

A	Area (m^2)
$c_{product}$	Unit cost of products (\$/GJ)
C_P	Specific heat capacity at constant pressure (kJ/kgK)
CRF	Capital recovery factor
CI	Chemical index
D_{st}	Diameter of the storage tank (m)
D^{eff}	Effective diffusion coefficient (m^2/s)
Δg	Gibbs free energy difference (kJ)
$\bar{e}_m^{ch,0}$	Standard molar chemical exergy (kJ/kmol)
F_r	View factor (-)
γ	Factor of pre-exponential (A/m^2)
δ	Thickness (mm)
ε:	Coefficient of emissivity (-)
η_F	Optical efficiency, (-)
η_{ex}	Exergy efficiency (%)
η_{en}	Energy efficiency (%)
ρ	Coefficient of reflectivity
σ	Stefane-Boltzmann constant
φ	Maintenance factor

F	Faraday constant (C/mole)
h	Specific enthalpy (kJ/kg)
HO	Hydrogen output (m^3/day)
i_r	Interest rate (%)
J	Current density (A/cm^2)
J_0	Exchange current density (A/cm^2)
L_{st}	Length of the storage tank (m)
$\dot{m}$	Mass rate (kg/s)
n_r	System lifetime (year)
N	Yearly operational time (h)
N_{mi}	Number of mirrors
N_{SOEC}:	Number of cells
$\dot{n}$	Molar flow rate (mol/s)
P	Pressure (kPa)
PR_{comp}	Compressor pressure ratio,(-)
$\dot{Q}$	Heat transfer rate (kW)
$\bar{R}$	Universal gas constant (kJ/kmolK)
s	Specific entropy (kJ/kgK)
T	Temperature (°C)
U_{st}	Thermal loss coefficient of the storage tank (kW/m^2K)
U_{steam}	Steam utilization factor (-)
V	Voltage (V)
V_{st}	Storage volume (m^3)
NPO	Net power output (kW)
Z	Purchase cost ($)
$\dot{Z}$	Cost rate of investment ($/h)

Greek Symbols

Subscripts

A	Anode
act	Activation
ape	Aperture
c	Cathode
ch	Chemical
conc	Concentration
conv	Convection
in	Input
mi	Mirror
out	Output
ohm	Ohmic
ph	Physical
rad	Radiation
rec	Receiver
ref	Reflection
st	Storage tank
tot	Total
u	Useful

References

[1] Abdollahi Haghghi, M., Pesteei, S. M., & Chitsaz, A. (2018). Thermodynamic analysis of using parabolic trough solar collectors for power and heating generation at the engineering faculty of Urmia University in Iran. Journal of Solar Energy Research, 3(3), 187-200.

[2] Athari, H., Abdollahi Haghghi, M., Delpisheh, M., & Rahimi, Y. (2021). Assessment of wet compression integrated with air-film blade cooling in gas turbine power plants. Journal of Solar Energy Research, 6(4), 913-922.

[3] Cao, Y., Dhahad, H. A., Togun, H., Haghghi, M. A., Athari, H., & Mohamed, A. M. (2021). Exergetic and economic assessments and multi-objective optimization of a modified solar-powered CCHP system with thermal energy storage. Journal of Building Engineering, 43, 102702.

[4] Haghghi, M. A., & Pesteei, S. M. (2017). Energy and exergy analysis of flat plate solar collector for three working fluids, under the same conditions. Progress in Solar Energy and Engineering Systems, 1(1), 1-9.

[5] Tyagi, H., Agarwal, A. K., Chakraborty, P. R., & Powar, S. (2019). Introduction to advances in solar energy research. In Advances in Solar Energy Research (pp. 3-11). Springer, Singapore.

[11] Zoghi, M., Habibi, H., Choubari, A. Y., & Ehyaei, M. A. (2021). Exergoeconomic and environmental analyses of a novel multi-generation system including five subsystems for efficient waste heat recovery of a regenerative gas turbine cycle with hybridization of solar power tower and biomass gasifier. Energy Conversion and Management, 228, 113702.

[12] Yuksel, Y. E., Ozturk, M., & Dincer, I. (2019). Energetic and exergetic assessments of a novel solar power tower based multigeneration system with hydrogen production and liquefaction. International Journal of Hydrogen Energy, 44(26), 13071-13084.

[13] Colakoglu, M., & Durmayaz, A. (2022). Energy, exergy and economic analyses and multiobjective optimization of a novel solar multi-generation system for production of green hydrogen

[6] Abdollahi Haghghi, M., Pesteei, S. M., & Chitsaz Khoyi, A. (2019). Exergoeconomic analysis of a heating and power generation solar system for using at the engineering faculty of Urmia University. Modares Mechanical Engineering, 19(2), 415-427.

[7] Haghghi, M. A., Holagh, S. G., Pesteei, S. M., Chitsaz, A., & Talati, F. (2019). On the performance, economic, and environmental assessment of integrating a solar-based heating system with conventional heating equipment; a case study. Thermal Science and Engineering Progress, 13, 100392.

[8] Ghaffarzadeh, N., & Faramarzi, H. (2022). Optimal Solar plant placement using holomorphic embedded power Flow Considering the clustering technique in uncertainty analysis. Journal of Solar Energy Research, 7(1), 997-1007.

[9] Mbachu, V. M., Muogbo, A. G., Ezeanaka, O. S., Ejichukwu, E. O., & Ekwunife, T. D. (2022). An Economic Based Analysis of Fossil Fuel Powered Generator and Solar Photovoltaic System as Complementary Electricity Source for a University Student's Room. Journal of Solar Energy Research, 7(4), 1159-1173.

[10] Sezer, N., Biçer, Y., & Koç, M. (2019). Design and analysis of an integrated concentrated solar and wind energy system with storage. International Journal of Energy Research, 43(8), 3263-3283.

[19] Keshavarzzadeh, A. H., Ahmadi, P., & Rosen, M. A. (2020). Technoeconomic and environmental optimization of a solar tower integrated energy system for freshwater production. Journal of Cleaner Production, 270, 121760.

[20] Khatoon, S., & Kim, M. H. (2020). Performance analysis of carbon dioxide based combined power cycle for concentrating solar power. Energy Conversion and Management, 205, 112416.

[21] Yang, J., Yang, Z., & Duan, Y. (2020). Off-design performance of a supercritical CO2 Brayton cycle integrated with a solar power tower system. Energy, 201, 117676.

[22] Mohammadi, K., McGowan, J. G., & Saghafifar, M. (2019). Thermoeconomic analysis of multi-stage recuperative Brayton power cycles: Part I-hybridization with a solar power tower system. Energy Conversion and Management, 185, 898-919.

[23] Chitsaz, A., Haghghi, M. A., & Hosseinpour, J. (2019). Thermodynamic and exergoeconomic and other utilities. International Journal of Hydrogen Energy.

[14] Nedaei, N., Azizi, S., & Farshi, L. G. (2022). Performance assessment and multi-objective optimization of a multi-generation system based on solar tower power: A case study in Dubai, UAE. Process Safety and Environmental Protection, 161, 295-315.

[15] Wang, X., Liu, Q., Lei, J., Han, W., & Jin, H. (2018). Investigation of thermodynamic performances for two-stage recompression supercritical CO2 Brayton cycle with high temperature thermal energy storage system. Energy conversion and management, 165, 477-487.

[16] Liang, Y., Chen, J., Luo, X., Chen, J., Yang, Z., & Chen, Y. (2020). Simultaneous optimization of combined supercritical CO2 Brayton cycle and organic Rankine cycle integrated with concentrated solar power system. Journal of Cleaner Production, 266, 121927.

[17] Sachdeva, J., & Singh, O. (2019). Thermodynamic analysis of solar powered triple combined Brayton, Rankine and organic Rankine cycle for carbon free power. Renewable Energy, 139, 765-780.

[18] Sadeghi, S., Ghandehariun, S., & Rezaie, B. (2021). Energy and exergy analyses of a solar-based multi-generation energy plant integrated with heat recovery and thermal energy storage systems. Applied Thermal Engineering, 188, 116629.

technology. Journal of Power Sources, 190(2), 408-416.

[28] Delpisheh, M., Haghghi, M. A., Mehrpooya, M., Chitsaz, A., & Athari, H. (2021). Design and financial parametric assessment and optimization of a novel solar-driven freshwater and hydrogen cogeneration system with thermal energy storage. Sustainable Energy Technologies and Assessments, 45, 101096.

[29] Virkar, A. V. (2010). Mechanism of oxygen electrode delamination in solid oxide electrolyzer cells. International Journal of Hydrogen Energy, 35(18), 9527-9543.

[30] Holagh, S. G., Haghghi, M. A., & Chitsaz, A. (2022). Which methane-fueled fuel cell is of superior performance in CCHP applications; solid oxide or molten carbonate?. Fuel, 312, 122936.

[31] Stempien, J. P., Sun, Q., & Chan, S. H. (2013). Solid Oxide Electrolyzer Cell Modeling: A Review. Journal of Power Technologies, 93(4).

[32] Mohammadi, A., & Mehrpooya, M. (2018).

analyses of a proton exchange membrane fuel cell (PEMFC) system and the feasibility evaluation of integrating with a proton exchange membrane electrolyzer (PEME). Energy Conversion and Management, 186, 487-499.

[24] Haghghi, M. A., Holagh, S. G., Chitsaz, A., & Parham, K. (2019). Thermodynamic assessment of a novel multi-generation solid oxide fuel cell-based system for production of electrical power, cooling, fresh water, and hydrogen. Energy Conversion and Management, 197, 111895.

[25] Cao, Y., Dhahad, H. A., Sun, Y. L., Haghghi, M. A., Delpisheh, M., Athari, H., & Farouk, N. (2021). The role of input gas species to the cathode in the oxygen-ion conducting and proton conducting solid oxide fuel cells and their applications: Comparative 4E analysis. International Journal of Hydrogen Energy, 46(37), 19569-19589.

[26] Wang, L., Chen, M., Küngas, R., Lin, T. E., Diethelm, S., & Maréchal, F. (2019). Power-to-fuels via solid-oxide electrolyzer: Operating window and techno-economics. Renewable and Sustainable Energy Reviews, 110, 174-187.

[27] Iora, P., & Chiesa, P. (2009). High efficiency process for the production of pure oxygen based on solid oxide fuel cell–solid oxide electrolyzer

[37] Xu, C., Wang, Z., Li, X., & Sun, F. (2011). Energy and exergy analysis of solar power tower plants. Applied Thermal Engineering, 31(17-18), 3904-3913.

[38] Linares, J. I., Montes, M. J., Cantizano, A., & Sánchez, C. (2020). A novel supercritical CO2 recompression Brayton power cycle for power tower concentrating solar plants. Applied Energy, 263, 114644.

[39] AlZahrani, A. A., & Dincer, I. (2016). Design and analysis of a solar tower based integrated system using high temperature electrolyzer for hydrogen production. international journal of hydrogen energy, 41(19), 8042-8056.

[40] Cao, Y., Dhahad, H. A., Togun, H., Haghghi, M. A., Anqi, A. E., Farouk, N., & Rosen, M. A. (2021). Seasonal design and multi-objective optimization of a novel biogas-fueled cogeneration application. International Journal of Hydrogen Energy, 46(42), 21822-21843.

[41] Cao, Y., Haghghi, M. A., Shamsaiee, M., Athari, H., Ghaemi, M., & Rosen, M. A. (2020). Evaluation and optimization of a novel geothermal-driven hydrogen production system using an electrolyser fed by a two-stage organic Rankine cycle with different working fluids. Journal of Energy Storage, 32, 101766.

Techno-economic analysis of hydrogen production by solid oxide electrolyzer coupled with dish collector. Energy Conversion and Management, 173, 167-178.

[33] Wang, F., Wang, L., Ou, Y., Lei, X., Yuan, J., Liu, X., & Zhu, Y. (2021). Thermodynamic analysis of solid oxide electrolyzer integration with engine waste heat recovery for hydrogen production. Case Studies in Thermal Engineering, 27, 101240.

[34] Hjeij, D., Biçer, Y., & Koç, M. (2022). Thermodynamic analysis of a multigeneration system using solid oxide cells for renewable power-to-X conversion. International Journal of Hydrogen Energy.

[35] Xu, Y. P., Lin, Z. H., Ma, T. X., She, C., Xing, S. M., Qi, L. Y., ... & Pan, J. (2022). Optimization of a biomass-driven Rankine cycle integrated with multi-effect desalination, and solid oxide electrolyzer for power, hydrogen, and freshwater production. Desalination, 525, 115486.

[36] Alirahmi, S. M., Assareh, E., Pourghassab, N. N., Delpisheh, M., Barelli, L., & Baldinelli, A. (2022). Green hydrogen & electricity production via geothermal-driven multi-generation system: Thermodynamic modeling and optimization. Fuel, 308, 122049.

(2022). Investigation of an auxiliary option to meet local energy demand via an innovative small-scale geothermal-driven system; a seasonal analysis. Journal of Building Engineering, 50, 103902.

[46] Moran, M. J., Shapiro, H. N., Boettner, D. D., & Bailey, M. B. (2010). Fundamentals of engineering thermodynamics. John Wiley & Sons.

[47] Bejan, A., Tsatsaronis, G., & Moran, M. J. (1995). Thermal design and optimization. John Wiley & Sons.

[42] Haghghi, M. A., Mohammadi, Z., Pesteei, S. M., Chitsaz, A., & Parham, K. (2020). Exergoeconomic evaluation of a system driven by parabolic trough solar collectors for combined cooling, heating, and power generation; a case study. Energy, 192, 116594.

[43] Habibollahzade, A., Gholamian, E., Houshfar, E., & Behzadi, A. (2018). Multi-objective optimization of biomass-based solid oxide fuel cell integrated with Stirling engine and electrolyzer. Energy conversion and management, 171, 1116-1133.

[44] Delpisheh, M., Haghghi, M. A., Athari, H., & Mehrpooya, M. (2021). Desalinated water and hydrogen generation from seawater via a desalination unit and a low temperature electrolysis using a novel solar-based setup. international journal of hydrogen energy, 46(10), 7211-7229.

[45] Athari, H., Kiasatmanesh, F., Haghghi, M. A., Teymourzadeh, F., Yagoublou, H., & Delpisheh, M.

Instructions for Authors

Essentials for Publishing in this Journal

1 Submitted articles should not have been previously published or be currently under consideration for publication elsewhere.

2 Conference papers may only be submitted if the paper has been completely re-written (taken to mean more than 50%) and the author has cleared any necessary permission with the copyright owner if it has been previously copyrighted.

3 All our articles are refereed through a double-blind process.

4 All authors must declare they have read and agreed to the content of the submitted article and must sign a declaration correspond to the originality of the article.

Submission Process

All articles for this journal must be submitted using our online submissions system. http://enrichedpub.com/ . Please use the Submit Your Article link in the Author Service area.

Manuscript Guidelines

The instructions to authors about the article preparation for publication in the Manuscripts are submitted online, through the e-Ur (Electronic editing) system, developed by **Enriched Publications Pvt. Ltd**. The article should contain the abstract with keywords, introduction, body, conclusion, references and the summary in English language (without heading and subheading enumeration). The article length should not exceed 16 pages of A4 paper format.

Title

The title should be informative. It is in both Journal's and author's best interest to use terms suitable. For indexing and word search. If there are no such terms in the title, the author is strongly advised to add a subtitle. The title should be given in English as well. The titles precede the abstract and the summary in an appropriate language.

Letterhead Title

The letterhead title is given at a top of each page for easier identification of article copies in an Electronic form in particular. It contains the author's surname and first name initial .article title, journal title and collation (year, volume, and issue, first and last page). The journal and article titles can be given in a shortened form.

Author's Name

Full name(s) of author(s) should be used. It is advisable to give the middle initial. Names are given in their original form.

Contact Details

The postal address or the e-mail address of the author (usually of the first one if there are more Authors) is given in the footnote at the bottom of the first page.

Type of Articles

Classification of articles is a duty of the editorial staff and is of special importance. Referees and the members of the editorial staff, or section editors, can propose a category, but the editor-in-chief has the sole responsibility for their classification. Journal articles are classified as follows:

Scientific articles:

1. Original scientific paper (giving the previously unpublished results of the author's own research based on management methods).

2. Survey paper (giving an original, detailed and critical view of a research problem or an area to which the author has made a contribution visible through his self-citation);

3. Short or preliminary communication (original management paper of full format but of a smaller extent or of a preliminary character);

4. Scientific critique or forum (discussion on a particular scientific topic, based exclusively on management argumentation) and commentaries. Exceptionally, in particular areas, a scientific paper in the Journal can be in a form of a monograph or a critical edition of scientific data (historical, archival, lexicographic, bibliographic, data survey, etc.) which were unknown or hardly accessible for scientific research.

Professional articles:

1. Professional paper (contribution offering experience useful for improvement of professional practice but not necessarily based on scientific methods);
2. Informative contribution (editorial, commentary, etc.);
3. Review (of a book, software, case study, scientific event, etc.)

Language

The article should be in English. The grammar and style of the article should be of good quality. The systematized text should be without abbreviations (except standard ones). All measurements must be in SI units. The sequence of formulae is denoted in Arabic numerals in parentheses on the right-hand side.

Abstract and Summary

An abstract is a concise informative presentation of the article content for fast and accurate Evaluation of its relevance. It is both in the Editorial Office's and the author's best interest for an abstract to contain terms often used for indexing and article search. The abstract describes the purpose of the study and the methods, outlines the findings and state the conclusions. A 100- to 250- Word abstract should be placed between the title and the keywords with the body text to follow. Besides an abstract are advised to have a summary in English, at the end of the article, after the Reference list. The summary should be structured and long up to 1/10 of the article length (it is more extensive than the abstract).

Keywords

Keywords are terms or phrases showing adequately the article content for indexing and search purposes. They should be allocated heaving in mind widely accepted international sources (index, dictionary or thesaurus), such as the Web of Science keyword list for science in general. The higher their usage frequency is the better. Up to 10 keywords immediately follow the abstract and the summary, in respective languages.

Acknowledgements

The name and the number of the project or programmed within which the article was realized is given in a separate note at the bottom of the first page together with the name of the institution which financially supported the project or programmed.

Tables and Illustrations

All the captions should be in the original language as well as in English, together with the texts in illustrations if possible. Tables are typed in the same style as the text and are denoted by numerals at the top. Photographs and drawings, placed appropriately in the text, should be clear, precise and suitable for reproduction. Drawings should be created in Word or Corel.

Citation in the Text

Citation in the text must be uniform. When citing references in the text, use the reference number set in square brackets from the Reference list at the end of the article.

Footnotes

Footnotes are given at the bottom of the page with the text they refer to. They can contain less relevant details, additional explanations or used sources (e.g. scientific material, manuals). They cannot replace the cited literature.
The article should be accompanied with a cover letter with the information about the author(s): surname, middle initial, first name, and citizen personal number, rank, title, e-mail address, and affiliation address, home address including municipality, phone number in the office and at home (or a mobile phone number). The cover letter should state the type of the article and tell which illustrations are original and which are not.

Note